JCB

Article

The actin-MRTF-SRF transcriptional circuit controls tubulin acetylation via *α-TAT1* gene expression

Jaime Fernández-Barrera,[1] Miguel Bernabé-Rubio,[1] Javier Casares-Arias,[1] Laura Rangel,[1,2] Laura Fernández-Martín,[1] Isabel Correas,[1,2] and Miguel A. Alonso[1]

[1]Department of Cell Biology and Immunology, Centro de Biología Molecular Severo Ochoa, Consejo Superior de Investigaciones Científicas and Universidad Autónoma de Madrid, Madrid, Spain
[2]Department of Molecular Biology, Universidad Autónoma de Madrid, Madrid, Spain

The role of formins in microtubules is not well understood. In this study, we have investigated the mechanism by which INF2, a formin mutated in degenerative renal and neurological hereditary disorders, controls microtubule acetylation. We found that silencing of INF2 in epithelial RPE-1 cells produced a dramatic drop in tubulin acetylation, increased the G-actin/F-actin ratio, and impaired myocardin-related transcription factor (MRTF)/serum response factor (SRF)–dependent transcription, which is known to be repressed by increased levels of G-actin. The effect on tubulin acetylation was caused by the almost complete absence of α-tubulin acetyltransferase 1 (α-TAT1) messenger RNA (mRNA). Activation of the MRTF-SRF transcriptional complex restored α-TAT1 mRNA levels and tubulin acetylation. Several functional MRTF-SRF–responsive elements were consistently identified in the *α-TAT1* gene. The effect of INF2 silencing on microtubule acetylation was also observed in epithelial ECV304 cells, but not in Jurkat T cells. Therefore, the actin-MRTF-SRF circuit controls *α-TAT1* transcription. INF2 regulates the circuit, and hence microtubule acetylation, in cell types where it has a prominent role in actin polymerization.

Introduction

Coordinated actions of the actin cytoskeleton and microtubule (MT) network are essential for several critical cellular processes, including formation of the leading edge and focal adhesions during cell migration, and of the intercellular bridge during cytokinesis (Green et al., 2012; Etienne-Manneville, 2013). The subset of MTs involved in these processes are often more stable than the bulk of MTs and typically accumulate a variety of posttranslational modifications (Wloga and Gaertig, 2010; Janke and Bulinski, 2011). Posttranslational modifications of tubulin are read by molecular motors and can be used to target them and their cargo to subpopulations of MTs that have been stabilized (Kreitzer et al., 1999; Lin et al., 2002; Reed et al., 2006; Dompierre et al., 2007; Konishi and Setou, 2009).

Although the majority of posttranslational modifications of tubulin are on the exterior of the MT, acetylation on the K40 residue of α-tubulin occurs in the MT lumen (Nogales et al., 1999) and could affect the binding of proteins that are transported along the interior of the MT (Burton, 1984; Garvalov et al., 2006; Bouchet-Marquis et al., 2007). Tubulin acetylation does not significantly change the ultrastructure of MTs or the conformation of tubulin (Howes et al., 2014), but it has been recently reported that α-tubulin acetylation weakens lateral interprotofilament interactions that enhance MT flexibility and thereby protect MTs from mechanical stress (Portran et al., 2017; Xu et al., 2017). In mammalian cells, tubulin acetylation marks MTs found in primary cilia, centrioles, a subset of cytoplasmic MT arrays, mitotic spindles, and intercellular cytokinetic bridges (Perdiz et al., 2011). Tubulin acetylation is important for early polarization events in neurons (Reed et al., 2006; Hammond et al., 2010), cell adhesion and contact inhibition of proliferation in fibroblasts (Aguilar et al., 2014), and touch sensation in *Caenorhabditis elegans* and mice (Shida et al., 2010; Kalebic et al., 2013; Kim et al., 2013; Aguilar et al., 2014; Morley et al., 2016). Increased tubulin acetylation has been observed in cystic kidney disease (Berbari et al., 2013), whereas decreased acetylation is linked to neurodegenerative disorders such as Alzheimer's, Huntington's, and Charcot-Marie-Tooth (CMT) diseases (Dompierre et al., 2007; Kazantsev and Thompson, 2008; d'Ydewalle et al., 2011; Qu et al., 2017). Despite its importance, the mechanism that regulates MT acetylation remains unknown.

Formins are a widely expressed family of proteins whose primary function is to nucleate monomeric globular actin (G-actin) to form linear filaments of actin (F-actin; Wallar and Alberts, 2003; Goode and Eck, 2007). In addition to their role in actin dynamics, formin functions affect the MT cytoskeleton (Goode and Eck, 2007; Bartolini and Gundersen, 2010; Chesarone et al., 2010). Most formins analyzed bind

Correspondence to Miguel A. Alonso: maalonso@cbm.csic.es

The Rockefeller University Press
J. Cell Biol. Vol. 217 No. 3 929–944
https://doi.org/10.1083/jcb.201702157

to MTs (Palazzo et al., 2001; Zhou et al., 2006; Bartolini et al., 2008; Young et al., 2008; Cheng et al., 2011; Gaillard et al., 2011), and the overexpression of deregulated fragments produces coalignment of MTs and actin filaments (Ishizaki et al., 2001), promotes MT stabilization (Palazzo et al., 2001), and induces tubulin acetylation (Copeland et al., 2004; Young et al., 2008; Thurston et al., 2012). Inverted formin 2 (INF2) was originally characterized as an atypical formin that, in addition to polymerizing actin, as other formins do, causes severing and disassembly of actin filaments in vitro. The latter two activities require the diaphanous autoregulatory domain (DAD), which in INF2 contains a Wiskott-Aldrich syndrome homology region 2 (WH2) motif that binds G-actin (Chhabra and Higgs, 2006). A second feature of INF2 is that the in vitro binding of G-actin to the WH2/DAD releases INF2 from its autoinhibitory state, thereby activating actin polymerization (Ramabhadran et al., 2013). INF2 regulates vesicular transport (Andrés-Delgado et al., 2010; Madrid et al., 2010), mitochondrial fission (Korobova et al., 2013; Manor et al., 2015), prostate cancer cell migration and invasion (Jin et al., 2017), focal adhesion elongation and maturation (Skau et al., 2015), and podosome formation and size (Panzer et al., 2016). It also remodels perinuclear actin in response to mechanical stimulation and increased intracellular calcium levels (Shao et al., 2015; Wales et al., 2016). Like other formins (Bartolini and Gundersen, 2010), INF2 binds to MTs (Gaillard et al., 2011; Bartolini et al., 2016) and promotes the formation of stabilized MT arrays (Andrés-Delgado et al., 2012; Bartolini et al., 2016), and its overexpression induces MT acetylation (Thurston et al., 2012). Mutations in the diaphanous inhibitory domain (DID) of INF2 have been found to cause focal segmental glomerulosclerosis (FSGS), a degenerative kidney disease, with or without associated CMT neuropathy (Brown et al., 2010; Boyer et al., 2011).

Given the importance and the specific regulatory properties of INF2, in this study we have investigated the impact of INF2 on tubulin acetylation. We show that INF2 knockdown (KD) or knockout (KO) causes a profound and general drop in tubulin acetylation in human retinal epithelial 1 (RPE-1) cells. Neither drugs that inhibit tubulin deacetylation nor those that increase MT stability were able to correct this effect. The lack of tubulin acetylation was accompanied by a dramatic decrease in the mRNA levels of α-tubulin acetyltransferase (α-TAT1), which is the enzyme responsible for α-tubulin acetylation (Shida et al., 2010; Kalebic et al., 2013; Kim et al., 2013; Aguilar et al., 2014), and by an increase in the G-/F-actin ratio. The exogenous expression of α-TAT1 restored tubulin acetylation in INF2-silenced cells. Further work revealed that the actin/myocardin–related transcription factor (MRTF)/serum response factor (SRF) transcriptional circuit, which is known to be repressed by increased levels of free G-actin (Posern and Treisman, 2006; Olson and Nordheim, 2010), controls *α-TAT1* transcription, and that INF2 influences tubulin acetylation by regulating this circuit. In addition to RPE-1 cells, INF2 was important for tubulin acetylation in epithelial ECV304 cells, but not in Jurkat T cells, indicating that INF2 regulates tubulin acetylation in a cell type–specific manner. Because MT abnormalities are thought to play a role in FSGS and FSGS plus CMT caused by INF2 mutations (Shaye and Greenwald, 2015), our demonstration that INF2 is crucial for tubulin acetylation in some types of cell may further our understanding of the molecular basis of these diseases.

Results

Tubulin acetylation is dramatically blocked in INF2 KD cells

The axoneme of primary cilia is formed by MTs that are extensively modified by acetylation of α-tubulin, facilitating the monitoring of this posttranslational MT modification. Tubulin acetylation is also very prevalent in the intercellular bridge formed during cytokinesis and, in interphase cells, in centrioles and specific MT arrays. To investigate the effect of INF2 silencing on MT acetylation, we generated RPE-1 cell clones with INF2 expression stably knocked down (INF2 KD cells) with specific shRNA (Fig. S1, A and B). Expression of Smo-GFP or staining of endogenous Arl13b, two ciliary membrane proteins, was used to visualize the cilium. It is of particular note that the percentage of cells with acetylated axonemes was greatly reduced in INF2 KD cells, whereas that of cells with polyglutamylated axonemes was unaffected (Fig. 1, A and B). The size of the cilia and the number of ciliated cells were unaffected by INF2 KD (Fig. S1, C and D). The analysis of a cell clone silenced with a different INF2 shRNA gave similar results (Fig. S1, E–H). Acetylation, but not polyglutamylation, of the MTs of the intercellular bridge formed during cytokinesis was compromised in INF2 KD cells (Fig. 1, C and D), as was the acetylation of centrioles (Fig. 1, E and F). Consistent with a general defect in MT acetylation, the cytoplasm of INF2 KD cells in interphase lacked detectable acetylated MT arrays (Fig. 1, G and H), although the organization of the MT cytoskeleton, as revealed by staining for α-tubulin, was normal (Fig. S1 I). The effect of INF2 KD on tubulin acetylation in RPE-1 cells was confirmed by assessing the levels of acetylated tubulin by immunoblot analysis (Fig. 1, I and J).

To investigate whether INF2 is required for tubulin acetylation in cell lines other than RPE-1 cells, we used CRISPR/Cas9 gene editing to prepare INF2 KO cell clones of epithelial ECV304 cells and Jurkat T cells. As control, we observed that INF2 KO in RPE-1 cells reproduced the results obtained with RPE-1 KD cells (Fig. S2, A–E). Although more than 50 candidates were examined, we did not obtain ECV304 cell clones with complete silenced expression of INF2, suggesting that the complete elimination of INF2 expression in this cell line might be deleterious. Consistent with the observations in RPE-1 cells, ECV304 cells with approximately half the content of INF2, which is probably the consequence of the KO of only one of the alleles, showed reduced tubulin acetylation (Fig. S2, F–J). In contrast, tubulin acetylation was unaffected in INF2 KO Jurkat T cell clones (Fig. S2, K–O). In conclusion, INF2 controls tubulin acetylation in RPE-1 and ECV304 cells but not in all cell types.

Absence of tubulin acetylation in INF2 KD cells is not caused by defects in MT stabilization or enhanced deacetylation

Tubulin acetylation accumulates in a subset of MTs that are more stable than the bulk of MTs. The accumulation of acetylated tubulin appears to be a consequence of the long duration of those MTs and not the cause of their stabilization (Palazzo et al., 2003). Cell treatment with MT-stabilizing drugs, such as taxol, promotes tubulin hyperacetylation (Piperno et al., 1987). To examine in detail the relationship between INF2 and tubulin acetylation, we used the RPE-1 cell line for subsequent experiments. First, we incubated cells in the presence or absence of

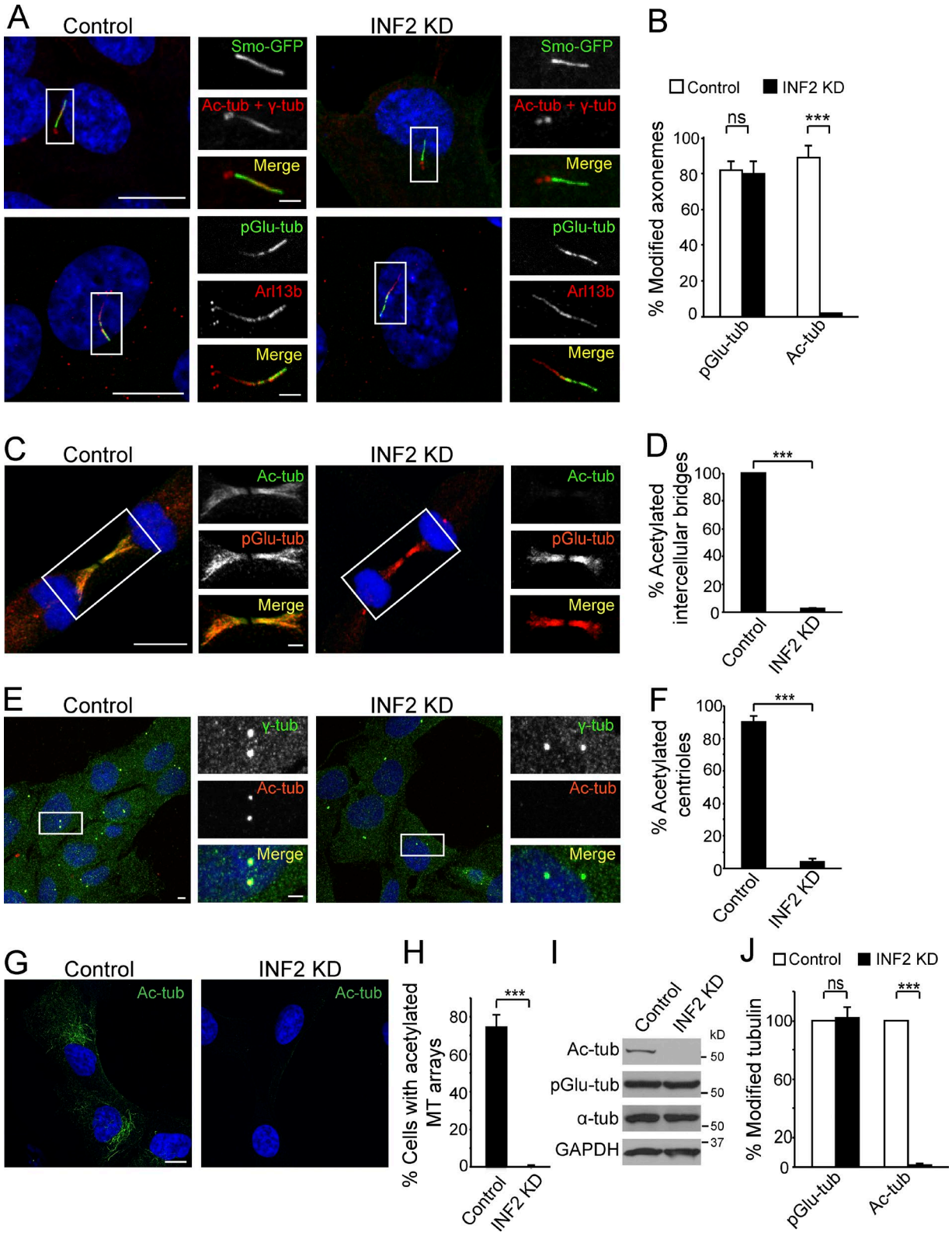

Figure 1. **INF2 KD produces a general block in α-tubulin acetylation in RPE-1 cells. (A and B)** Control or INF2 KD cells expressing Smo-GFP (top) or not (bottom) were stained for acetylated tubulin (Ac-tub) and γ-tubulin (γ-tub) in the same fluorescence channel (top) or for polyglutamylated tubulin (pGlu-tub) and endogenous Arl13b (bottom). Smo-GFP and Arl13b were used to visualize the ciliary membrane (A). **(B)** The number of primary cilia positive for pGlu-tub or Ac-tub in control and INF2 KD cells was quantified and expressed as the percentage of the total number of primary cilia examined (n = 300–450 per experimental point). **(C and D)** Control and INF2 KD cells were stained for Ac-tub and pGlu-tub. Only cells in cytokinesis are shown (C). **(D)** The number of control and INF2 KD cells with the intercellular bridge stained for acetylated tubulin was quantified and expressed as the percentage of the total numbers of bridges examined (n = 300–400 cells per experimental point). **(E and F)** To visualize the centrioles, control or INF2 KD cells were treated with 10 µM nocodazole for 2 h at room temperature, followed by an additional 30 min at 4°C. Cells were fixed with cold methanol for 6 min. Cells were finally

taxol for 3 h and stained them for acetylated tubulin to determine whether the lack of tubulin acetylation in INF2 KD cells is caused by defective MT stabilization. Cells were scored as MT hyperacetylated cells when the level of MT acetylation, as determined by measuring the signal intensity of the labeling, was at least three times that of the mean level of control cells. Using this criterion, fewer than 5% of control cells showed hyperacetylated MTs. In contrast to the high percentage of MT-hyperacetylated cells observed in the case of control cells treated with taxol, no effect in tubulin acetylation was detected in taxol-treated INF2 KD cells (Fig. 2, A and B). This result was confirmed by immunoblotting (Fig. 2, C and D). Tubacin is known to increase the levels of tubulin acetylation by inhibiting histone deacetylase 6 (HDAC6), which deacetylates MTs (Haggarty et al., 2003). To investigate whether the deficiency in tubulin acetylation is caused by enhanced deacetylation by HDAC6, we treated control and INF2 KD RPE-1 cells with tubacin or with its inactive analogue, niltubacin. As expected, the percentage of cells with hyperacetylated MTs increased in control cells treated with tubacin, whereas no effect was observed in INF2 KD cells (Fig. 2, E and F). The lack of effect of tubacin on tubulin acetylation in INF2 KD cells was confirmed by immunoblotting (Fig. 2, G and H). Together, the results in Fig. 2 suggest that the lack of tubulin acetylation in INF2 KD RPE-1 cells is not a consequence of defective MT stabilization or enhanced tubulin deacetylation.

INF2 KD cells are depleted of α-TAT1 mRNA

A possible explanation of the deficiency of tubulin acetylation is that the expression of α-TAT1 is reduced in INF2 KD RPE-1 cells. Because we did not find any reliable source of antibodies to detect endogenous α-TAT1, we measured the expression of α-TAT1 mRNA by quantitative PCR. It is of note that, consistent with the acetylation defects observed in INF2 KD cells, we found α-TAT1 mRNA levels to be greatly reduced in INF2 KD cells compared with control cells (Fig. 3 A). To confirm that the lack of α-TAT1 is responsible for the lack of acetylation in INF2 KD cells, we expressed α-TAT1-GFP to restore tubulin acetylation in these cells. We observed that expression of α-TAT1-GFP, but not of its α-TAT1 D157N-GFP mutant, which has only residual catalytic activity (Shida et al., 2010), produced tubulin hyperacetylation in all the transfected cells (Fig. 3 B). This result was confirmed by assessing the levels of acetylated tubulin by immunoblot analysis (Fig. 3, C and D). The results in Fig. 3 indicate that the defect in tubulin acetylation observed in INF2 KD cells was caused by the lack of α-TAT1 expression.

Tubulin acetylation is restored in INF2 KD cells by expression of catalytically active INF2 fragments

Most formins consist of a carboxyl-terminal domain, known as the DAD, which is separated by formin homology (FH) domains 1–2 from the DID, which is at the amino terminus. The FH1 domain recruits profilin, which binds and supplies G-actin to the FH2 domain for actin polymerization (Wallar and Alberts, 2003; Goode and Eck, 2007). INF2 is expressed as two isoforms, INF2-1 and INF2-2, generated by alternative splicing of the exons encoding their carboxyl-terminal end (Fig. 4 A). INF2-1, which has an 18-aa carboxyl-terminal sequence containing a motif for farnesylation, localizes to the ER, whereas INF2-2, which instead has a 9-aa sequence containing basic residues, is cytosolic (Madrid et al., 2010; Ramabhadran et al., 2011). The I643 residue, which is present in the FH2 domain of human INF2, is critical for actin polymerization in vivo (Ramabhadran et al., 2012). This residue is equivalent to the I1431 of yeast formin Bni1p and the I704 of mDia2, which are critical for actin polymerization by these formins (Xu et al., 2004; Harris et al., 2006). However, K792 in the FH2 of human INF2, which is equivalent to a K residue critical for actin polymerization by Bni1p (K1601) and mDia2 (K853; Xu et al., 2004; Bartolini et al., 2008), is not essential for actin polymerization by INF2 (Ramabhadran et al., 2012). On the other hand, mutation of three critical leucine residues (L1010, L1011 and L1020) in the DAD of mouse INF2, equivalent to L976, L977, and L986 in human INF2, abrogates the in vitro depolymerization activity of INF2 (Chhabra and Higgs, 2006; Chhabra et al., 2009).

We expressed intact human INF2 (INF2-1 and INF2-2) or INF2 proteins with I643 (INF2-1 IA and INF2-2 IA), K792 (INF2-1 KA), or L976, 977, 986 (INF2-1 3LA) substituted by Ala (Fig. S3 A) and assayed their ability to induce tubulin hyperacetylation in control RPE-1 cells. Whereas the KA and 3LA mutants were as active as intact INF2, the IA mutants showed a reduced effect (Fig. 4, B and C; and Fig. S3 B). All the INF2 proteins distributed throughout the cell (Figs. 4 B and S3 B), except for the INF2-1 IA mutant, which accumulated in collapsed membranous structures that correspond to a modified ER, as indicated by its colocalization with mCherry-ER-3, an ER marker (Fig. S3 C). The reduced effect of the IA mutation on tubulin hyperacetylation was confirmed by expression of an INF2 IA mutant with the alternative carboxyl-terminal sequence deleted (INF2 IA ΔAlt; Fig. 4, B and C; and Fig. S3 A).

We also expressed intact INF2 or different INF2 fragments to analyze their capacity to restore tubulin acetylation in INF2 KD cells (Fig. 4, D and E; and Fig. S3 D). Intact INF2-2 and the fragment consisting of the FH1-FH2 domains induced tubulin acetylation and so did the FH2 domain, although to a lesser extent. The activity of INF2 and its FH2 fragment promoting tubulin acetylation was abolished by the mutation of the I643 residue (Fig. 4, D and E), which also blocks its actin polymerization activity (Ramabhadran et al., 2012). It is of note that INF2-2 IA induced a significant increase in the percentage of cells with hyperacetylated tubulin in control cells (Fig. 4, B and C), but had no effect in INF2 KD cells (Figs. 4 E and S3 E). This finding indicates that INF2 overexpression regulates tubulin acetylation in control cells by mechanisms that are dependent on and independent of its actin

stained separately for Ac-tub and γ-tub (E). **(F)** The number of centrioles positive for Ac-tub in control and INF2 KD cells was quantified and expressed as the percentage of the total number of centrioles examined (n = 300–400 cells per experimental point). **(G and H)** Control and INF2 KD cells were stained for Ac-tub. Only cells in interphase are shown (G). (H) The number of control and INF2 KD cells with acetylated MT arrays was quantified and expressed as the percentage of the total number of cells examined (n = 300–350 cells per experimental point). In A, C, E, and G, nuclei were visualized with TO-PRO. Enlargements of the boxed regions are shown. **(I and J)** Total extracts from control or INF2 KD cells were subjected to immunoblot analysis for Ac-tub, pGlu-tub, total α-tubulin (α-tub), and GAPDH (I). **(J)** The histogram shows the levels of Ac-tub and pGlu-tub in INF2 KD cells relative to those in control cells. Bars: (panoramic views) 10 µm; (enlargements) 2 µm. Data in B, D, F, H, and J represent the mean and SEM of three independent experiments; ns, not significant; ***, $P < 0.001$.

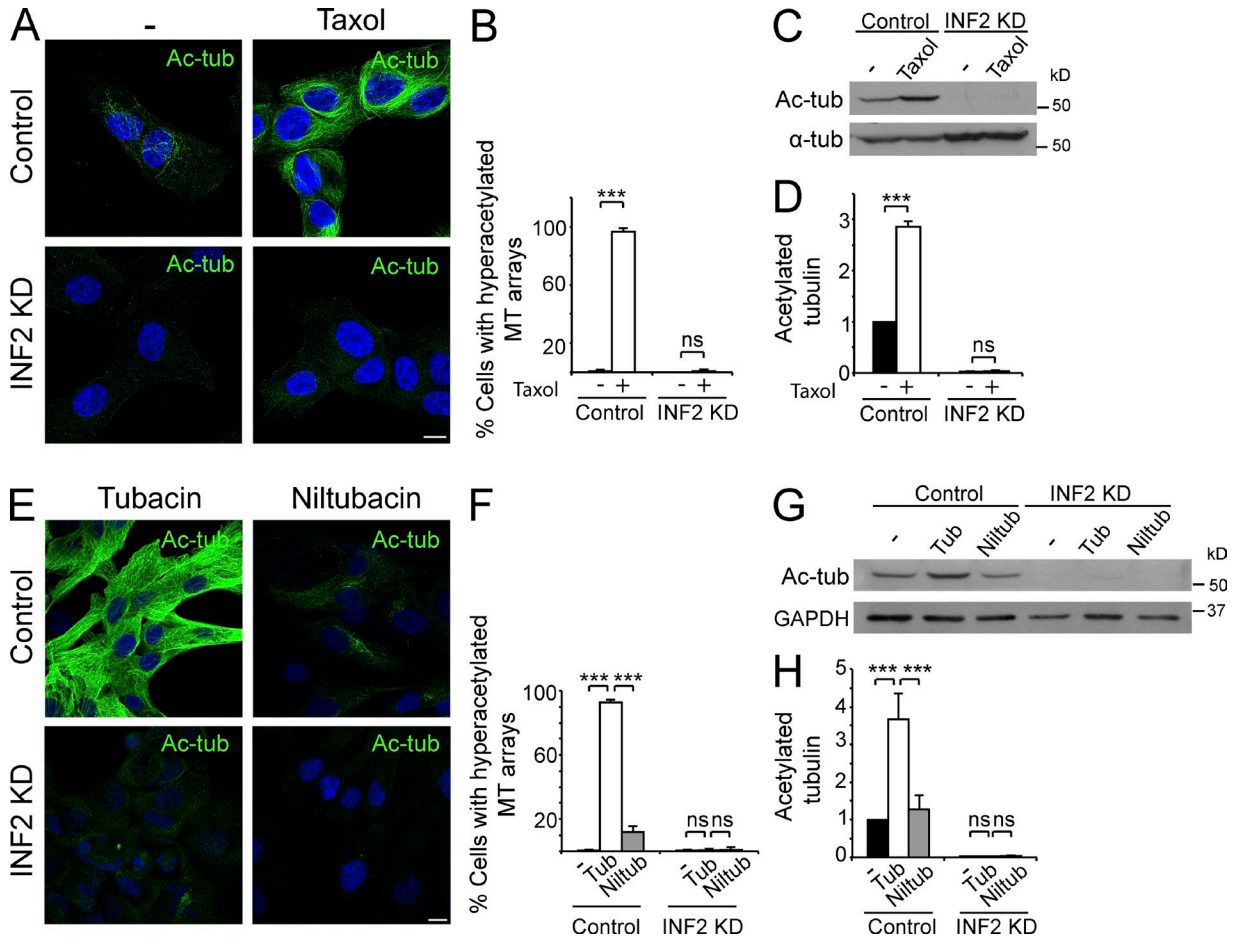

Figure 2. **Absence of tubulin acetylation in INF2 KD cells is not caused by defects in MT stabilization or enhanced deacetylation. (A–D)** Control and INF2 KD RPE-1 cells were left untreated or were treated with 2.5 µM taxol for 2 h and stained for Ac-tub (A). **(B)** The number of cells with hyperacetylated MTs was determined and expressed as the percentage of the total number of cells examined (n = 420–450 cells per experimental point). **(C)** Cell extracts were subjected to immunoblot analysis for Ac-tub and total α-tub. **(D)** The histogram shows the levels of Ac-tub relative to those in untreated control cells. **(E–H)** Control and INF2 KD cells were treated with 10 µM of either tubacin or niltubacin for 8 h and stained for Ac-tub (E). **(F)** The number of cells with hyperacetylated MT arrays was determined and expressed as the percentage of the total number of cells examined (n = 350–450 cells per experimental point). **(G)** Cell extracts were subjected to immunoblot analysis for Ac-tub and GAPDH. **(H)** The histogram shows the levels of Ac-tub in INF2 KD cells relative to those in untreated control cells. Nuclei were visualized with TO-PRO in A and E. Bars, 10 µm. Data in B, D, F, and H represent the mean and SEM of three independent experiments; ns, not significant; ***, $P < 0.001$.

polymerization activity, the independent mechanism probably being mediated by MT stabilization. However, in INF2 KD cells, only an actin polymerization activity–dependent mechanism operates. The stable expression of either INF2-1 or INF2-2 in INF2 KO cells restored tubulin acetylation, indicating that both isoforms probably help regulate the expression of the *α-TAT1* gene (Fig. S3, F–H). The results illustrated in Fig. 4 highlight the importance of the FH2 domain of INF2 and its actin polymerization activity for promoting tubulin acetylation in RPE-1 cells.

DIA1 KD does not inhibit tubulin acetylation or alter the G-/F-actin ratio, unlike INF2 KD

To ascertain whether all the formins are equally important for MT acetylation in RPE-1 cells, we knocked down the expression of DIA1 (DIA1 KD cells), which is the human orthologue of mouse Dia1 (mDia1; Li and Higgs, 2003), with specific shRNA (Fig. 5, A and B). We found that the percentage of cells with acetylated MT arrays and the levels of α-TAT1 mRNA were unaffected in DIA1 KD cells (Fig. 5, C–E). It is of note that DIA1 KD had no significant effect on the G-/F-actin ratio, whereas INF2 KD greatly increased it (Fig. 5 F). In conclusion, INF2 appears to have a more prominent role than DIA1 in actin polymerization and tubulin acetylation in RPE-1 cells.

Despite the lack of effect of DIA1 KD on tubulin acetylation, the overexpression of mDia1-GFP, constitutive active mDia1 ΔN3-GFP mutant, or the isolated FH2 domain of mDia1 (Fig. S4 A) promoted tubulin acetylation in INF2 KD cells (Fig. 5, G and H). The same effect was obtained by overexpression of the formin FMNL1 or its isolated FH2 domain (Fig. 5 H and Fig. S3, I and J). The actin polymerization activity of mDia1 is abolished by the substitution of three critical lysine residues (K989, K994, and K999) by alanine (mDia FH2 KA3; Ishizaki et al., 2001). We expressed the FH2 fragment of mDia1 with the KA3 mutation and found that, unlike the intact fragment, it was unable to restore tubulin acetylation in INF2 KD cells (Fig. 5, G and H). These results, together with those in Fig. 4, indicate that the overexpression of FH2-containing fragments corrects the tubulin acetylation defect of INF2 KD RPE-1 cells, and does so only when their actin polymerization activity is preserved.

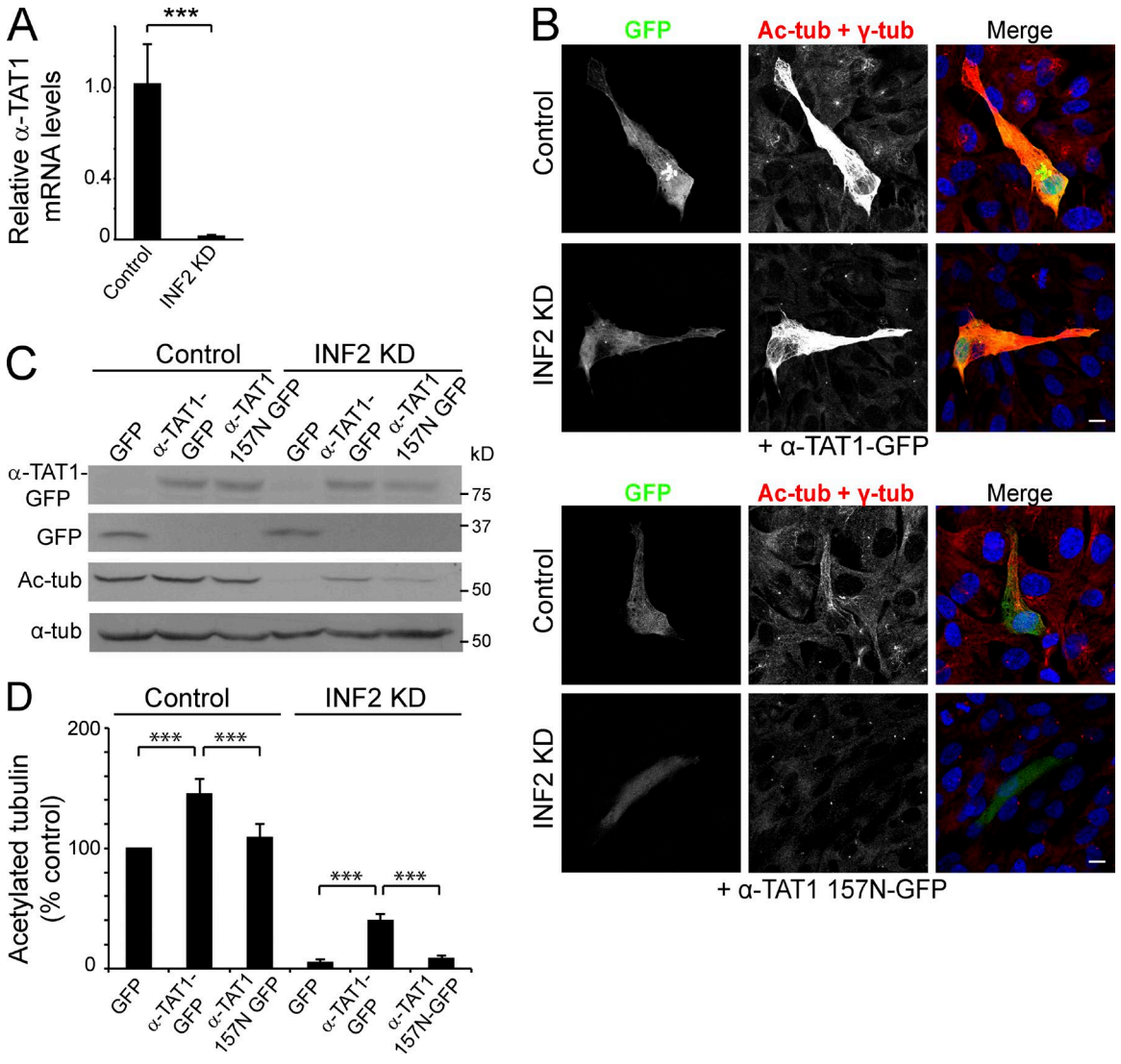

Figure 3. **INF2 KD cells are depleted in α-TAT1 mRNA. (A)** The histogram represents the levels of α-TAT1 mRNA in INF2 KD cells relative to those in control RPE-1 cells. **(B)** Control and INF2 KD cells were transiently transfected with α-TAT1-GFP (top) or α-TAT1 157N-GFP (bottom) and stained for Ac-tub and γ-tub in the same fluorescence channel. Nuclei were visualized with TO-PRO. Bars, 10 µm. **(C and D)** Total extracts from control or INF2 KD cells transiently expressing GFP, α-TAT1-GFP, or α-TAT1 157N-GFP were subjected to immunoblot analysis with antibodies to GFP and for Ac-tub and total α-tub. The same blot was cut in strips and processed to detect GFP alone, α-TAT1-GFP and α-TAT1 157N-GFP, or Ac-tub (C). **(D)** The histogram shows the percentage of Ac-tub in cells expressing α-TAT1-GFP and α-TAT1 157N-GFP relative to that in control cells transfected with GFP alone. Data in A and D represent the mean and SEM of three independent experiments; ***, $P < 0.001$.

Activation of the actin-MRTF-SRF transcriptional circuit restores α-TAT1 mRNA levels and tubulin acetylation in INF2 KD cells

SRF is a highly conserved and widely expressed transcription factor in mammals (Prywes and Roeder, 1987; Treisman, 1987). MRTF coactivators, which regulate SRF activity by forming a complex with SRF, are regulated by the levels of cytoplasmic and nuclear G-actin (Miralles et al., 2003; Baarlink et al., 2013). The requirement for actin polymerization activity to restore MT acetylation in INF2 KD cells (Fig. 4, D and E) is consistent with the possibility that the actin-MRTF-SRF circuit regulates MT acetylation. The transcriptional activity of MRTF-SRF complex was assayed with a luciferase reporter plasmid (5xCArG) containing five canonical MRTF-SRF–responsive elements upstream from a minimal promoter. When we compared control and INF2 KD RPE-1 cells, we found that the transcriptional activity of the MRTF-SRF complex is reduced in INF2 KD cells (Fig. 6 A). To confirm the reduction in MRTF-SRF transcriptional activity, we evaluated the mRNA levels of several known MRTF-SRF transcriptional targets involved in focal adhesions, such as the genes encoding the extracellular matrix connective tissue growth factor and the cytoskeletal proteins α-actinin 1, filamin A, talin 1, tropomyosin 1, and vinculin. We found a significant reduction in the levels of the mentioned transcripts to an extent that is consistent with the drop in MRTF-SRF activity observed in INF2 KD cells (Fig. 6 B). Compared with *α-TAT1* (Fig. 3 A), the effect was more moderate, suggesting that the transcription of these genes at steady-state is less dependent on the MRTF-SRF complex.

The amino terminus of MRTFs contains a RPEL domain that binds five G-actin molecules, resulting in the sequestration of the MRTF molecules in the cytosol (Guettler et al., 2008). When levels of cytosolic G-actin are low, MRTF is imported into

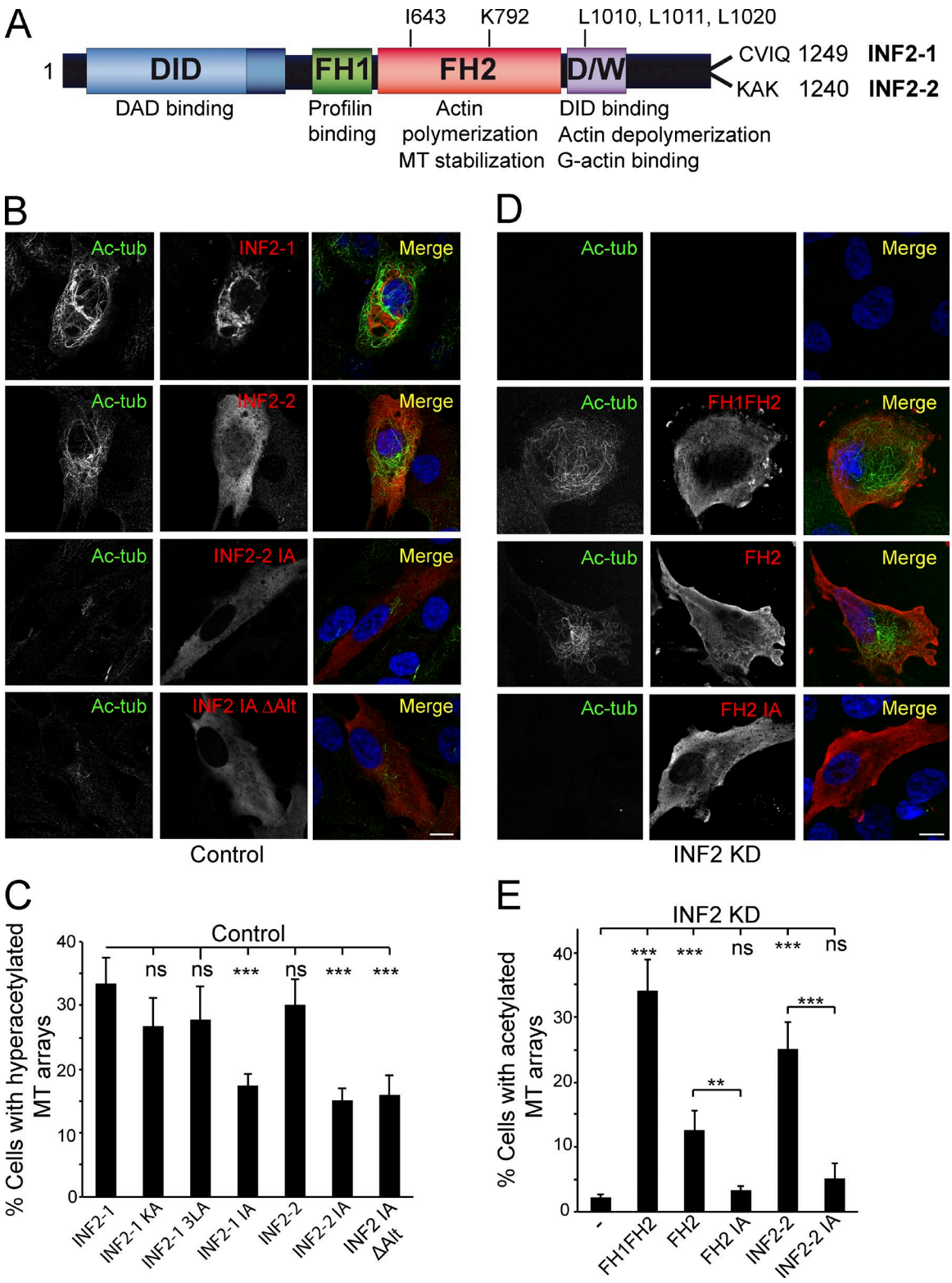

Figure 4. **Expression of an intact FH2 domain restores tubulin acetylation in INF2 KD cells. (A)** Schematic of the domain organization of INF2. The position of the amino acids mutated in the different constructs used and the carboxyl-terminal amino acid sequence of INF2-1 and INF2-2 as well as the function of the different domains are indicated. D/W, DAD/WH2 domain. **(B and C)** Control RPE-1 cells transiently expressing the indicated INF2 proteins were stained for Ac-tub and exogenous INF2 (B). **(C)** The histogram shows the percentage of cells transfected with the indicated constructs showing MT hyperacetylation. Fewer than 5% of the control cells showed hyperacetylated MTs. **(D and E)** INF2 KD RPE-1 cells were left untransfected or were transiently transfected with the indicated INF2 constructs. Cells were stained for Ac-tub and the exogenous INF2 fragments (D). **(E)** The histogram illustrates the percentage of INF2 KD cells transfected with the indicated constructs showing MT acetylation. Nuclei were visualized with TO-PRO in B and D. Bars, 10 µm. Data in C and E represent the mean and SEM of three independent experiments (n = 300–400 cells per experimental point); ns, not significant; **, $P < 0.01$; ***, $P < 0.001$.

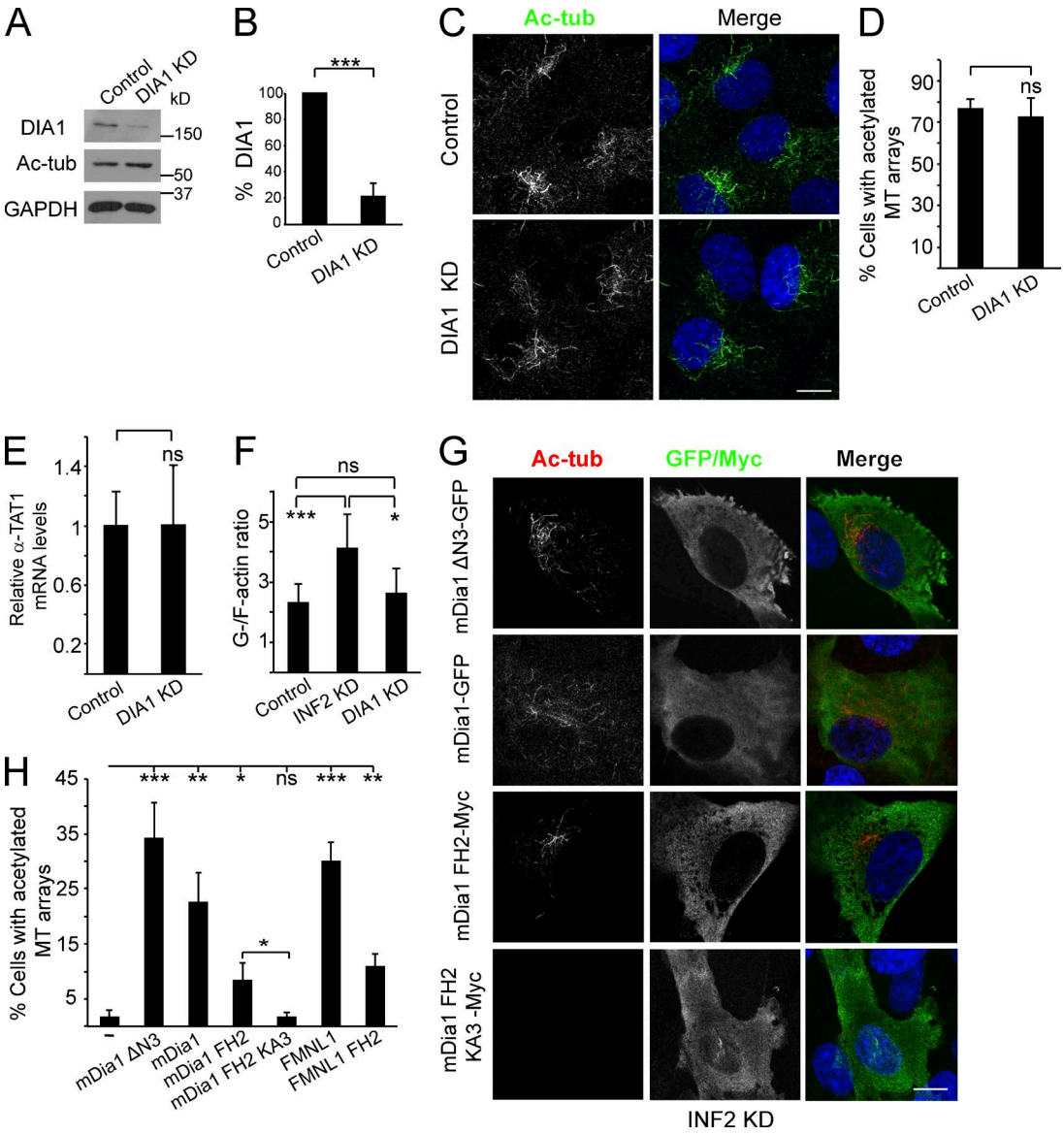

Figure 5. **INF2 KD but not DIA1 KD alters the G-/F-actin ratio. (A and B)** Extracts from control or RPE-1 cells stably expressing shRNA targeted to DIA1 (DIA1 KD) were immunoblotted for DIA1, Ac-tub, and GAPDH (A). **(B)** The histogram represents the levels of DIA1 in DIA1 KD cells relative to control cells. **(C and D)** Control or DIA1 KD cells were stained for Ac-tub (C). **(D)** The number of control and DIA1 KD cells with acetylated MT arrays was quantified and as the percentage of the total number of cells examined (n = 350–450 cells per experimental point). **(E)** The histogram represents the levels of α-TAT1 mRNA in DIA1 KD cells relative to control cells. **(F)** The G-/F-actin ratio was determined in control cells, INF2 KD cells, and DIA1 KD cells. **(G)** INF2 KD cells transiently expressing tagged forms of full-length mDia1, the mDia1 ΔN3 mutant, and the intact or KA3 mutant of the FH2 domain of mDia1 were stained for Ac-tub and the exogenous proteins. **(H)** The histogram shows the percentage of cells with acetylated MT arrays in INF2 KD cells expressing the mDia1 constructs indicated in (G), full-length FMNL1, or the FMNL1 FH2 domain (n = 300–400 cells per experimental point). Nuclei were visualized with TO-PRO in C and G. Bars, 10 µm. Data in B, D, and H represent the mean and SEM of three independent experiments, and those in E and F represent five and seven independent experiments, respectively; ns, not significant; *, $P < 0.05$; **, $P < 0.01$; ***, $P < 0.001$.

the nucleus and associates with SRF to direct SRF-dependent gene transcription. Depletion of G-actin by either stimulation of F-actin formation or sequestration of G-actin liberates MRTFs from G-actin and allows the nuclear import of MRTF (Posern and Treisman, 2006; Olson and Nordheim, 2010). Cytochalasin D treatment not only disrupts the MRTF/G-actin complex, liberating MRTF (Olson and Nordheim, 2010), but also induces primary cilium formation by a mechanism that is yet to be fully characterized (Kim et al., 2010). Cytochalasin D increased the percentage of cells with acetylated axoneme and induced axoneme hyperacetylation in control cells (Fig. S4, A–C); in INF2 KD cells, it restored MRTF-SRF-dependent transcription (Fig. 6 A) and axoneme acetylation (Fig. 6, C and D) and increased the total levels of acetylated tubulin (Fig. 6, E and F) and α-TAT1 mRNA (Fig. 6 G).

Two related MRTFs, MRTF-A and MRTF-B, have been identified in mammalian species (Olson and Nordheim, 2010). To investigate the involvement of MRTF directly, we analyzed the levels of MRTF-A in the nucleus and found that they were significantly higher in control cells than in INF2 KD cells (Fig. 7, A and B). As control, we observed that the total levels of MRTF-A and SRF were similar in control and INF2 KD RPE-1 cells (Fig. S4 D). It is of particular note that treatment with cytochalasin D altered the distribution of MRTF-A

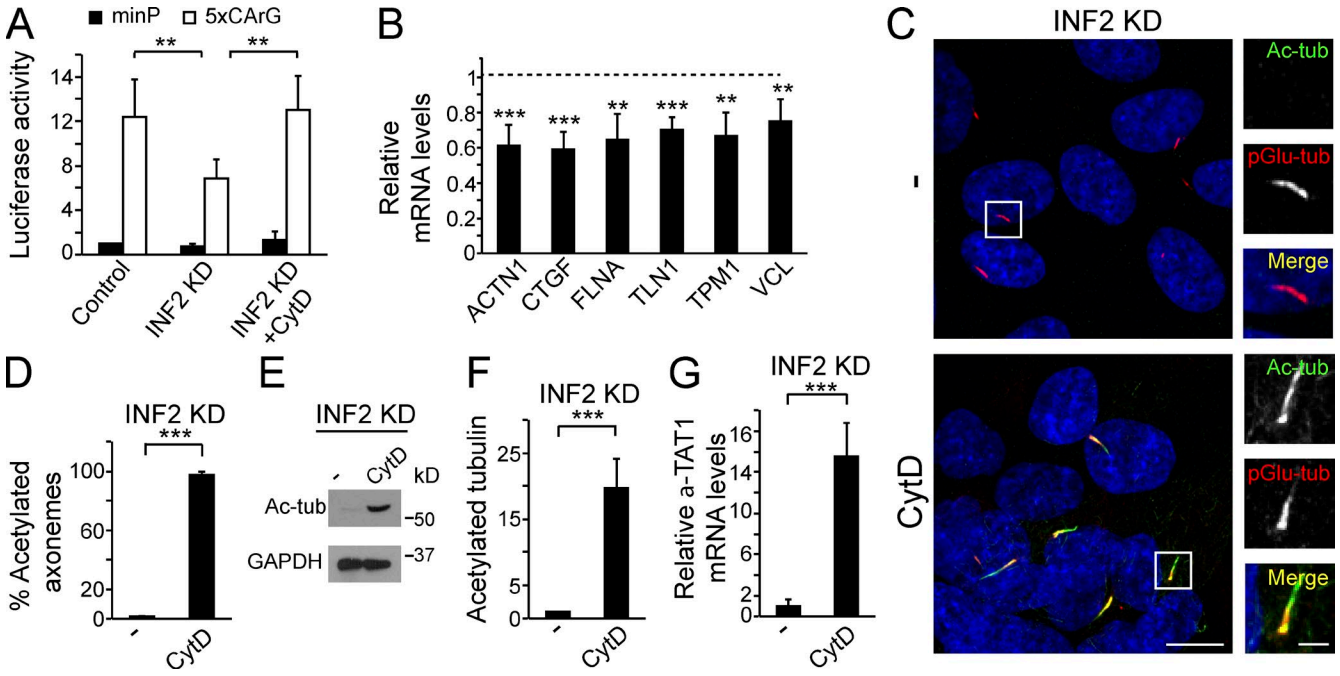

Figure 6. **The activity of the MRTF-SRF transcriptional complex is defective in INF2 KD RPE-1 cells. (A)** Control or INF2 KD RPE-1 cells were transfected with plasmids containing the luciferase reporter gene with a minimal promoter (minP) or five canonical CArG boxes followed by the minimal promoter (5xCArG). The activity of the MRTF-SRF complex was measured in control cells, INF2 KD cells, and cytochalasin D–treated INF2 KD cells. The values are expressed relative to those obtained in control cells transfected with minP. **(B)** The histogram illustrates the mRNA levels of α-actinin 1 (ACTN1), connective tissue growth factor (CTGF), filamin A (FLNA), talin 1 (TLN1), tropomyosin 1 (TPM1), and vinculin (VCL) in INF2 KD cells relative to that in control RPE-1 cells. The dashed line indicates the values in control cells. **(C and D)** INF2 KD cells were treated with 0.5 µM cytochalasin D or not for 48 h and stained for Ac-tub and pGlu-tub. Note that cytochalasin D treatment promotes the formation of primary cilia. Nuclei were visualized with DAPI. Enlargements of the boxed regions are shown. Bars: (panoramic views) 10 µm; (enlargements) 2 µm (C). (D) The histogram represents the percentage of axonemes, as visualized by pGlu-tub staining, that were acetylated (n = 365–383 cells per experimental point). **(E and F)** Total extracts from INF2 KD cells treated or not with cytochalasin D were immunoblotted for Ac-tub or GAPDH (E). **(F)** The histogram shows the levels of Ac-tub in cytochalasin D–treated INF2 KD cells relative to those in untreated cells. **(G)** The level of α-TAT1 mRNA in INF2 KD cells treated with cytochalasin D was quantified and expressed relative to that in untreated cells. Data in A and G represent the mean and SEM of six and four independent experiments, respectively; those in B, D, and F represent the mean and SEM of five independent experiments; **, P < 0.01; ***, P < 0.001.

in INF2 KD cells, making it mostly nuclear as in the control cells, with a concomitant increase in the percentage of INF2 KD cells with acetylated tubulin (Fig. 7, A and B). To further demonstrate a role of MRTF in regulating tubulin acetylation, we overexpressed the MRTF-A ΔN100 mutant, which lacks the amino-terminal 100 aa of MRTF-A containing the RPEL domain that binds G-actin and consequently displays constitutive activity (Muehlich et al., 2008). Confirming the role of MRTF, we found that MRTF-A ΔN100 expression restored tubulin acetylation in INF2 KD cells (Fig. 7, C and D). Consistent with our hypothesis that MRTF-SRF controls *α-TAT1* gene expression, MRTF-A ΔN100 overexpression activated MRTF-SRF–mediated gene transcription (Fig. 7 E) and increased α-TAT1 mRNA levels in INF2 KD cells (Fig. 7 F). To further demonstrate the involvement of MRTF in α-TAT1 expression, we used the pan-formin inhibitor SMIFH2 (Rizvi et al., 2009). The treatment of control RPE-1 cells with SIMFH2 produced the exclusion of endogenous MRTF-A from the nucleus and a dramatic reduction in the percentage of cells with acetylated MT arrays (Fig. S4, E and F). It is of note that, consistent with our results showing the crucial role of MRTF in promoting tubulin acetylation, this effect was partially overcome by the expression of MRTF-A ΔN100 (Fig. S4, E and F). In conclusion, the actin-MRTF-SRF circuit is dysfunctional in INF2 KD RPE-1 cells, and the activation of this circuit corrects the defect in tubulin acetylation.

The MRTF-SRF complex directly controls transcription of the *α-TAT1* gene

Homodimeric SRF recognizes 10-bp DNA elements called CArG boxes (Posern and Treisman, 2006). These are classified into two broad categories, consensus CArG boxes, which fit the sequence $CC(A/T)_6GG$ (Leung and Miyamoto, 1989); and CArG-like boxes, which include elements that do not deviate more than 1 bp from the consensus sequences (Sun et al., 2006). We inspected the human form of *α-TAT1* gene for putative CArG and CArG-like elements in the promoter region and the first intron. We found one consensus CArG box (CArG1), which was perfectly palindromic, and two CArG-like boxes (CArG2 and CArG3) in the promoter region and one CArG-like box in the first intron (CArG4; Fig. 8 A). To investigate whether the MRTF-SRF complex mediates transcription of the *α-TAT1* gene directly, we cloned three DNA fragments encompassing the indicated elements (Prom1, Prom2, and Int1; Fig. 8 A) upstream of a minimal promoter followed by the luciferase gene reporter (Fig. 8 B). The constructs were transfected in control and INF2 KD RPE-1 cells, and their luciferase activity was assayed. In control cells, we observed a marked increase in luciferase activity in all cases in response to incubation with 20% FBS compared with the cells transfected with the plasmid containing the minimal promoter alone. In contrast, the effect was reduced in INF2 KD cells (Fig. 8 B), as had been previously observed for the 5xCArG construct (Fig. 6 A). To confirm that

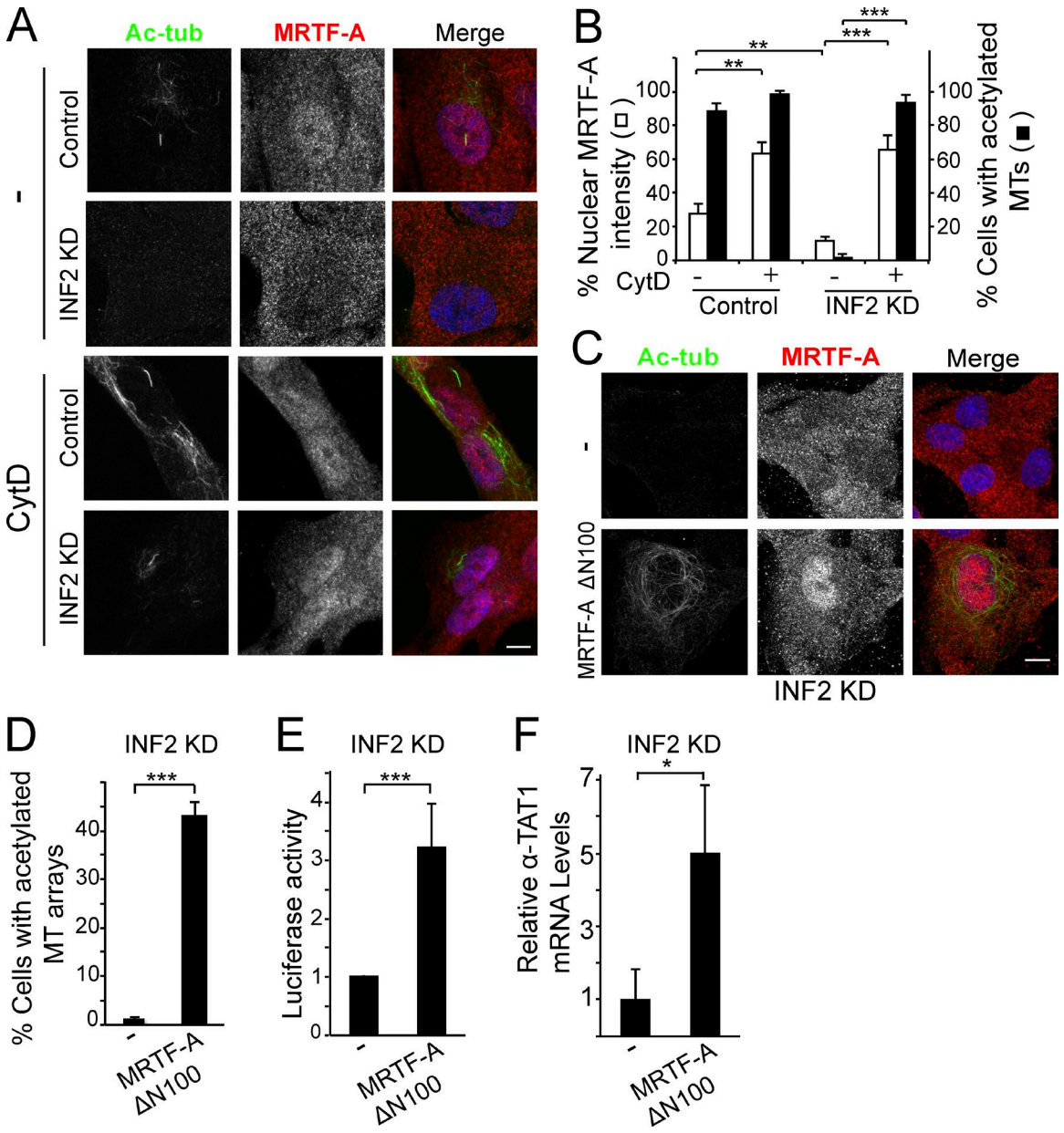

Figure 7. **Expression of active MRTF-A restores tubulin acetylation and α-TAT mRNA levels in INF2 KD RPE-1 cells. (A and B)** Control and INF2 KD RPE-1 cells were treated with 0.5 µM cytochalasin D or not for 48 h. Cells were then stained for Ac-tub and endogenous MRTF-A (A). **(B)** The percentage of nuclear MRTF-A and that of cells with acetylated MT arrays were quantified (n = 300–450 cells per experimental point). **(C–F)** INF2 KD cells expressing the active MRTF-A ΔN100 mutant or not were stained for MRTF-A and Ac-tub (C). **(D)** The percentage of transfected cells with acetylated MT arrays was quantified and compared with that of untransfected cells. **(E)** The activity of the MRTF-SRF complex was measured in INF2 KD cells expressing MRTF-A ΔN100 and expressed relative to that in untransfected INF2 KD cells. **(F)** The level of α-TAT1 mRNA was quantified in MRTF-A ΔN100-transfected INF2 KD cells and expressed relative to those in untransfected cells. Nuclei were visualized with TO-PRO in A and C. Bars, 10 µm. Data in B, D, and E represent the mean and SEM of four independent experiments; those in F represent the mean and SEM of three independent experiments; *, $P < 0.05$; **, $P < 0.01$; ***, $P < 0.001$.

these elements respond to MRTF-SRF activation, we cloned the four *α-TAT1* gene CArG elements in tandem (CArGs1–4 construct) and measured the luciferase activity in cells expressing the active MRTF-A ΔN100 mutant (Figs. 8 C and S4 G). The activity of CArGs1-4 was similar to that of the 5xCArG construct, whereas mutation in the central residues of each of the *α-TAT1* gene CArGs (CArGs1–4m construct) greatly reduced its activity. The results presented in Fig. 8 indicate that the *α-TAT1* gene contains CArG elements that respond to activation of the MRTF-SRF transcriptional complex.

Discussion

Lysine acetylation of α-tubulin was first reported more than 30 years ago (L'Hernault and Rosenbaum, 1985), with K40 being identified as the acetylation site (LeDizet and Piperno, 1987). K40 acetylation is the most extensively characterized of the known tubulin posttranslational modifications (Perdiz et al., 2011). The function of formins affects the actin and MT cytoskeletons (Goode and Eck, 2007; Bartolini and Gundersen, 2010; Chesarone et al., 2010). Despite the interest aroused, the

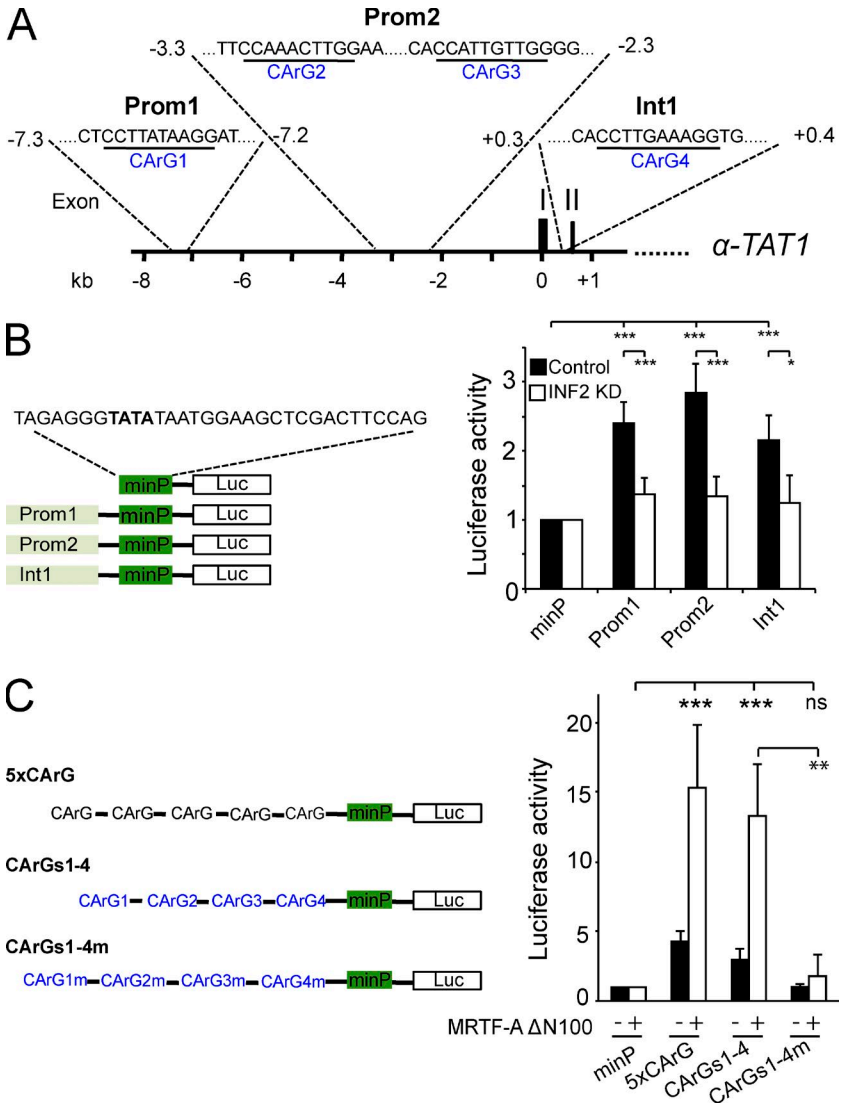

Figure 8. **The α-TAT1 gene contains functional CArG boxes. (A)** Schematic representation of the *α-TAT1* gene with an indication of the putative CArG boxes (CArG elements 1–4) present in the region examined and the fragments (Prom1, Prom2, and Int1) used in our analysis. **(B)** The indicated constructs were transfected in control and INF2 KD RPE-1 cells. The luciferase activity was measured and was expressed relative to that of cells transfected with minP. **(C)** The four CArG boxes present in the constructs Prom1, Prom2, and Int1 were placed in tandem upstream from a minimal promoter (α-TAT1 CArGs1–4). A similar construct was made in which the four central nucleotides of each box were mutated in such a way that all of them were C or G (α-TAT1 CArGs1–4m). Control cells were transfected with the indicated constructs in the presence or absence of the MRTF-A ΔN100 construct, and the luciferase activity of the cells was assayed. The histogram represents the luciferase activity obtained in each case relative to that of cells transfected with minP. Data in B and C represent the mean and SEM of seven and four independent experiments, respectively; ns, not significant; *, P < 0.05; **, P < 0.01; ***, P < 0.001.

mechanism by which formins regulate tubulin acetylation has remained puzzling. In this study, we have investigated how the formin INF2 controls MT acetylation. We observed that INF2 KD in RPE-1 cells produced a global defect in MT acetylation and an increase in the G-/F-actin ratio. The defect in tubulin acetylation was not caused by decreased MT stability or increased tubulin deacetylation. It is explained by the almost complete absence of α-TAT1 mRNA, which encodes the major tubulin acetyltransferase (Shida et al., 2010; Kalebic et al., 2013). Tubulin acetylation was restored by exogenous expression of α-TAT1 and treatments that induce activation of MRTF-SRF–dependent transcription, which is controlled by the levels of free monomeric G-actin. Several MRTF-SRF–responsive elements were identified as being responsible for the transcription of the *α-TAT1* gene. In conclusion, the actin-MRTF-SRF transcriptional circuit regulates *α-TAT1* gene expression, and INF2 affects MT acetylation in RPE-1 cells by regulating the transcription of the *α-TAT1* gene through this circuit.

Overexpression of deregulated FH1FH2-containing fragments from 13 mammalian formins induces to a greater or lesser extent tubulin acetylation and activation of MRTF-SRF–dependent transcription (Tominaga et al., 2000; Copeland and Treisman, 2002; Copeland et al., 2004; Young et al., 2008; Thurston et al., 2012). No absolute correlation was found between the tubulin acetylation and MRTF-SRF activation, which, in some cases, had a high level for one but a low level for the other. In addition, in the case of the formin INF1, the expression of its MT binding carboxyl-terminal domain induces tubulin acetylation but does not modify the activity of the MRTF-SRF complex (Young et al., 2008; Thurston et al., 2012). We have observed that the overexpression of the actin polymerization-deficient INF2 IA caused tubulin hyperacetylation in a population of control cells. This effect was probably caused by an increase in MT stability (Andrés-Delgado et al., 2012; Bartolini et al., 2016), because MT stabilization by formins is independent of actin polymerization (Bartolini et al., 2008). The effect of overexpressing intact INF2 was greater because, in addition, it can polymerize actin and activate transcription by the MRTF-SRF complex. Consistent with these observations, we noted that the overexpression of intact INF2-2 or the INF2 FH2 fragment produced an increase in tubulin acetylation in INF2 KD cells. However, INF2-2 IA or the INF2 FH2 IA mutant prompted no such increase because INF2 KD is depleted in α-TAT1. Based on our results and those earlier studies, we propose that formins affect tubulin acetylation by both stabilizing MTs and activating the transcription of the *α-TAT1* gene, although, depending on the

specific formin, one of the mechanisms dominates the other. For instance, in the case of endogenous INF2, the effect on *α-TAT1* gene transcription appears to be more important than that on MT stabilization, although the latter can also contribute. In INF2, as in most formins, these two activities require the presence of the FH2 domain, whereas in the formin INF1 they are segregated into different domains: the amino-terminal half containing the FH1 and FH2 domains moderately activates MRTF-SRF–dependent transcription and does not stabilize MTs, whereas its large carboxyl-terminal half, which contains the tubulin-binding region, is a potent MT stabilizer but does not activate the MRTF-SRF complex (Young et al., 2008). The case of formin Fmn1, which has a bipartite amino-terminal MT binding region segregated from its FH1 and FH2 domains (Zhou et al., 2006), could be similar to that of INF1.

INF2 mutations account for 10–15% of the cases of autosomal-dominant FSGS (Brown et al., 2010; Barua et al., 2013) and ∼75% of those of FSGS combined with CMT (Boyer et al., 2011). It is of particular note that whereas most discussions of defects underlying kidney disease and neuropathy for patients with INF2-related syndromes focus on the role of INF2 in modulating the actin cytoskeleton, studies conducted in *C. elegans* with disease-associated INF2 mutations point to an effect of mutant INF2 on both MTs and actin (Shaye and Greenwald, 2015). The MRTF-SRF complex is known to regulate the transcription of a large number of genes that encode regulators of the cytoskeleton, transcription, and cell growth and metabolism. Among the cytoskeleton genes regulated by MRTF-SRF are genes involved in actin dynamics, cell adhesion, extracellular matrix synthesis and processing, and cell motility and genes involved in MT-based cytoskeletal dynamics (Esnault et al., 2014; Gualdrini et al., 2016). Consequently, changes in INF2 activity in RPE-1 cells can control actin homeostasis and modulate the expression of *α-TAT1* and a large number of other genes related to cytoarchitecture that are regulated by the actin-MRTF-SRF transcriptional circuit. Therefore, INF2 can control not only tubulin acetylation, but also more extensive cytoskeleton remodeling, as has been observed in the cases of dorsal stress fibers and fibrillar focal adhesion formation (Skau et al., 2015), and in perinuclear actin remodeling in response to mechanical force (Shao et al., 2015).

As is the case with RPE-1 cells, INF2 appears to be important for tubulin acetylation in ECV304 cells. However, tubulin acetylation in Jurkat T cells is controlled by another mechanism. Because the regulation of transcription by the MRTF-SRF by free G-actin is probably universal in mammalian cells, it is possible that the CArG elements in the *α-TAT1* gene are not functional in all types of cells or that G-actin homeostasis is regulated in a different manner, by INF2 in certain cell types and, for instance, by another formin more prominent than INF2 in actin polymerization in others. In conclusion, our findings shed new light on the coordination of the actin cytoskeleton and MTs. This may help explain the molecular basis of INF2-related disease (Brown et al., 2010; Boyer et al., 2011) and the alterations in tubulin acetylation observed in other human disorders (Li and Yang, 2015).

Materials and methods

Antibodies and reagents

The rabbit polyclonal antibodies to INF2 (used at 1/2,000 for immunofluorescence analysis to detect only exogenous INF2 and at 1/500 for immunoblotting) have been described previously (Madrid et al., 2010). The sources of commercial antibodies to the indicated proteins were as follows: γ-tubulin (rabbit polyclonal; used at 1/1,000 for immunofluorescence analysis; T3559; and mouse mAb IgG1; used at 1/5,000 for immunofluorescence analysis; clone GTU-88, T6557), total α-tubulin (mouse mAb IgG1; used at 1/2,000 for immunoblotting; clone DM1A; T9026), and acetylated tubulin (mouse mAb IgG2b; used at 1/700 or 1/2,500 for immunofluorescence analysis of tubulin acetylation or hyperacetylation, respectively, and 1/2,000 for immunoblotting; clone 6-11B-1; T7451) were from Sigma-Aldrich; polyglutamylation modification (mouse mAb IgG1; used at 1/1,000 for immunofluorescence analysis and 1/1,000 for immunoblotting; clone GT335; AG-20B-0020) was from Adipogen*;* DIA1 (mouse mAb IgG1; used at 1/100 for immunoblotting; clone 51/mDia1; 610848) was from BD Transduction Labs; Arl13b (rabbit polyclonal, used at 1/1,000 for immunofluorescence analysis, 17711-1-AP) and MRTF-A (rabbit polyclonal; used at 1/100 for immunofluorescence analysis and 1/1,000 for immunoblotting; 21166-1-AP) were from Proteintech; SRF (rabbit polyclonal; used at 1/200 for immunoblotting; G-20, sc-335) was from Santa Cruz Biotechnology; Gapdh (mouse mAb IgG1; used at 1/5,000 for immunoblotting; clone 6C5, AM4300) was from Ambion. Taxol (paclitaxel), nocodazol, and cytochalasin D were from Sigma-Aldrich. SMIFH2 (1-(3-bromophenyl)-5-(2-furylmethylene)-2-thioxo-hexahydropyrimidine-4,6-dione; 344092) was from Merck. Tubacin and niltubacin were from Enzo Life Sciences. The TO-PRO-3 (T3605) and DAPI (268298) stains were from Thermo Fisher Scientific and Merck, respectively. Fluorescent phalloidin and secondary antibodies conjugated to Alexa Fluor 488, 555, 594, or 647 were from Life Technologies. HRP-conjugated secondary antibodies were from Jackson ImmunoResearch.

Cell culture conditions

Telomerase-immortalized human pigment epithelial cells RPE-1 (CRL-4000; ATCC) were grown in DMEM/F12 with 10% FBS, and ECV304 cells (CRL-1998; ATCC) and Jurkat T cells (TIB-152; ATCC) in DMEM with 10% FBS. Cells were incubated at 37°C in an atmosphere of 5% CO_2/95% air. Primary cilium formation in RPE-1 cells was induced by starving the cells in DMEM/F12 with 0.25% FBS for 24 h.

DNA constructs and transfection conditions

The plasmids expressing shRNAa or shRNAb specific to human INF2 used to generate the stable INF2 KD and INF2 KD2 cell clones, respectively, were made in the pSR-GFP/neo vector (Oligoengine) as described previously (Andrés-Delgado et al., 2010; Madrid et al., 2010). For DIA1 KD, we expressed shRNA specific to DIA1 cloned in the pLKO.1 puro vector (NM_005219.2-2523s1c1; Sigma-Aldrich). For CRISPR/Cas9 *INF2* gene editing, the INF2 cDNA sequence was analyzed using the Breaking-Cas tool (http://bioinfogp.cnb.csic.es/tools/breakingcas), and the target sequence selected (5′-CGGAGATAC GTGCAACGCCGCGG-3′) was inserted in the pSpCas9(BB)-2A-GFP plasmid (plasmid 48138; Addgene; Ran et al., 2013), which was a gift from F. Zhang (Massachusetts Institute of Technology, Cambridge, MA). GFP-positive cells were sorted after 48 h of transfection and plated. Individual clones were finally screened by immunoblotting and immunofluorescence analysis with antibodies to INF2. The DNA constructs expressing untagged full-length INF2 proteins with an intact or mutated amino acid sequence were cloned in the pCR3.1 DNA vector (Invitrogen). The DNA constructs expressing mDia1 and mDia1 ΔN3 fused to GFP (Ishizaki et al., 2001) were gifts from S. Narumiya (Kyoto University, Kyoto, Japan), and that expressing FMNL1-GFP (Seth et al., 2006) was donated by M.K. Rosen (University of Texas Southwestern Medical Center, Dallas, TX). The plasmids expressing wild-type α-TAT1 (plasmid 27099; Addgene) and inactive α-TAT1

Δ157N fused to GFP (plasmid 27100; Addgene; Shida et al., 2010) were gifts from M.V. Nachury (Stanford University, Stanford, CA); GFP-Smoothened (plasmid 25395; Addgene; Chen et al., 2002), and the MRTF-A ΔN100 mutant (plasmid 19848; Addgene; Muehlich et al., 2008) were gifts from P. Beachy (Johns Hopkins University, Baltimore, MD) and Ron Prywes (Columbia University, New York, NY), respectively; mCherry-ER-3 (plasmid 55041; Addgene) was a gift from M. Davidson (The Florida State University, Tallahassee, FL). The DNA constructs expressing INF2 deletion proteins (FH1FH2, FH2, and IA ΔAlt) as well as those expressing the isolated FH2 domain of mDia1 and FMNL1 were obtained by PCR and cloned in pCR3.1. Point mutations were introduced using the Quick-Change kit (Stratagene). All the constructs were verified by DNA sequencing (Macrogen). Cells were transfected with Lipofectamine 2000 (Invitrogen). RPE-1 cell clones stably expressing shRNA to INF2 or DIA1 were generated by transfection and selection with 0.5 mg/ml G-418 or 1 µg/ml puromycin, respectively. The resulting individual clones were trypsinized in situ with the help of stainless steel cloning cylinders, and the cells were plated onto coverslips and plastic dishes. Finally, the clones were screened by immunofluorescence and immunoblot analyses.

Confocal microscopic analysis

Cells were fixed in 4% PFA for 20 min, rinsed, and treated with 10 mM glycine for 5 min to quench the aldehyde groups. The cells were permeabilized with methanol at –20°C for 5 min, rinsed, and incubated with 3% BSA in PBS for 15 min. In the case of Arl13b staining, cells were permeabilized with 0.2% Triton X-100. Cells were then incubated for 1 h with the appropriate primary antibodies, rinsed several times, and incubated for 30 min with the appropriate combination of fluorescent secondary antibodies. Actin filaments were detected with phalloidin-Alexa Fluor 647. Coverslips were mounted with Fluoromount (Sigma-Aldrich). Controls to assess labeling specificity included incubations with, or omitting, control primary antibodies. Images were obtained at room temperature using the following confocal equipment: LSM510 coupled to an inverted Axiovert 200 microscope; LSM710 equipment coupled to an AxioImager.M2 microscope; a multiphoton LSM710 coupled to an AxioObserver microscope (Zeiss); 63×/1.4 oil Plan Apochromat and 100×/1.3 oil Plan Neofluar objectives were used. Images were analyzed with Fiji imaging software. Images were exported in TIFF format, and their brightness and contrast were optimized with Adobe Photoshop.

Transcription reporter assays

The pGL4.3.4[*luc2P*]/SRF-RE/Hygro vector (E1350; Promega) contains a sequence of five consensus CArG boxes in tandem separated by nucleotide spacers followed by a minimal promoter upstream of a modified firefly luciferase gene (5xCArG). This vector was used to generate derivatives with the CArG boxes removed (minP construct) or replaced by the indicated DNA fragments located upstream of the first exon (Prom1 and Prom 2 construct) or at the first intron (Int1 construct) of the human *α-TAT1* gene. To generate the plasmid α-TAT1 CArGs1-4, the sequence containing the five consensus CArG boxes of the pGL4.3.4[*luc2P*]/SRF-RE/Hygro vector was substituted by a synthetic sequence containing the CArG 1–4 boxes present in Prom1, Prom2, and Int1 but maintaining the nucleotide spacers of the vector. The construct α-TAT1 CArGs1-4m was made by mutation of the CArG elements in the α-TAT1 CArGs construct in such a way that the four central nucleotides of each element were G or C. The DNA constructs (150 ng) were transfected in RPE-1 cells together with 50 ng of a *Renilla* luciferase reporter plasmid, which was used to normalize the results for the efficiency of the transfection, using Lipofectamine 2000. After being starved for 20 h in culture medium with 0.5% FBS, cells were incubated with either 20% FBS or 500 nM cytochalasin D and were lysed 6 h afterward. Firefly and *Renilla* luciferase activity, which was used as a control of the transfection efficiency, was measured in a Sirius tube luminometer (Titertek Berthold) using a Dual-Luciferase reporter assay system (E1910; Promega). Each experiment was performed in triplicate.

Quantitative RT-PCR

Total RNA from RPE-1 cells was purified using RNeasy (74104; Qiagen). mRNA levels were analyzed by quantitative RT-PCR procedures using the Super Script III First-Strand Synthesis SuperMix kit (PN 11752250; Life Technologies) and the qPCR FAST Sybr Green PCR Master Mix kit (PN 4367659; Applied Biosystems) in an ABI 7900HT apparatus. The results were normalized with respect to the expression of Gapdh mRNA in the same samples. As indicated in the corresponding figure legend, three to five independent experiments were performed in triplicate. Data were analyzed with GenEX software. The oligonucleotide primers used for quantitative PCR are listed in Table S1.

Measurement of the G-/F-actin ratio and immunoblot analysis

The G-/F-actin ratio was determined using a commercial G-/F-actin in vivo assay kit strictly following the manufacturer's protocol (BKO37; Cytoskeleton). For immunoblotting, samples were subjected to SDS-PAGE and transferred onto nitrocellulose membranes (Amersham). After blocking with 5% nonfat dried milk powder and 0.05% Tween-20 in PBS, blots were incubated overnight with the appropriate antibodies. After several washes, blots were incubated for 30 min with secondary antibodies coupled to HRP. The signal was visualized with ECL chemiluminescence detection reagent (Thermo Fisher Scientific). Band intensities were quantified using ImageJ software, and results were expressed relative to the control condition.

Statistical analysis

Data are expressed as group means and SEM. *t* test for independent samples was used to establish the statistical significance of differences between group means.

Online supplemental material

Fig. S1 shows the effect of INF2 KD on the percentage of ciliated cells and the size of the cilia, and the effect of a second shRNA to INF2 on tubulin acetylation. Fig. S2 shows the effect of INF2 KO on tubulin acetylation in various cell lines. Fig. S3 shows representative images of the effect of the overexpression of INF2 mutants on tubulin acetylation in control RPE-1 cells and an immunoblot analysis of the expression of mDia1 and FMNL1 proteins in INF2 KD cells. Fig. S4 shows the effect of cytochalasin D on tubulin acetylation in control cells and the effect of MRTF-A Δ-N100 expression on tubulin acetylation in SMIFH2-treated cells. Table S1 shows the sequence of the primers used in the quantitative analysis of the expression of the various mRNAs examined.

Acknowledgments

The expert technical advice of the Optical and Confocal Microscopy and Genomics Units of the Centro de Biología Molecular Severo Ochoa (CBMSO) is gratefully acknowledged. We are grateful to Dr. Rosa M. Ríos (Centro Andaluz de Biología Molecular y Medicina Regenerativa), Dr. Jaime Millán, Dr. Ilenia Bernascone, Minerva Bosch, and Leticia Labat (CBMSO) and María Maroto (Centro Nacional de Investigaciones Oncológicas) for their helpful comments. We also thank Dr. Phil Mason for revising the English language of the manuscript.

This work was supported by a grant from the Spanish Ministerio de Economía y Competitividad (MINECO)/Fondo Europeo de

Desarrollo Regional (BFU2015-67266-R to M.A. Alonso. Contracts from the Ministerio de Educación, Cultura y Deporte (J. Fernández-Barrera and J. Casares-Arias) and MINECO (M. Bernabé-Rubio) are also acknowledged.

The authors declare no competing financial interests.

Author contributions: J. Fernández-Barrera performed the majority of the experiments and did the quantitative data analysis. M. Bernabé-Rubio, J. Casares-Arias, L. Rangel, and L. Fernández-Martín performed part of the immunofluorescence experiments. I. Correas and M.A. Alonso designed the experiments and supervised the work. M.A. Alonso conceived the project and wrote the manuscript.

Submitted: 24 February 2017
Revised: 28 June 2017
Accepted: 11 December 2017

References

Aguilar, A., L. Becker, T. Tedeschi, S. Heller, C. Iomini, and M.V. Nachury. 2014. A-tubulin K40 acetylation is required for contact inhibition of proliferation and cell-substrate adhesion. *Mol. Biol. Cell.* 25:1854–1866. https://doi.org/10.1091/mbc.E13-10-0609

Andrés-Delgado, L., O.M. Antón, R. Madrid, J.A. Byrne, and M.A. Alonso. 2010. Formin INF2 regulates MAL-mediated transport of Lck to the plasma membrane of human T lymphocytes. *Blood.* 116:5919–5929. https://doi.org/10.1182/blood-2010-08-300665

Andrés-Delgado, L., O.M. Antón, F. Bartolini, A. Ruiz-Sáenz, I. Correas, G.G. Gundersen, and M.A. Alonso. 2012. INF2 promotes the formation of detyrosinated microtubules necessary for centrosome reorientation in T cells. *J. Cell Biol.* 198:1025–1037. https://doi.org/10.1083/jcb.201202137

Baarlink, C., H. Wang, and R. Grosse. 2013. Nuclear actin network assembly by formins regulates the SRF coactivator MAL. *Science.* 340:864–867. https://doi.org/10.1126/science.1235038

Bartolini, F., and G.G. Gundersen. 2010. Formins and microtubules. *Biochim. Biophys. Acta.* 1803:164–173.

Bartolini, F., J.B. Moseley, J. Schmoranzer, L. Cassimeris, B.L. Goode, and G.G. Gundersen. 2008. The formin mDia2 stabilizes microtubules independently of its actin nucleation activity. *J. Cell Biol.* 181:523–536. https://doi.org/10.1083/jcb.200709029

Bartolini, F., L. Andres-Delgado, X. Qu, S. Nik, N. Ramalingam, L. Kremer, M.A. Alonso, and G.G. Gundersen. 2016. An mDia1-INF2 formin activation cascade facilitated by IQGAP1 regulates stable microtubules in migrating cells. *Mol. Biol. Cell.* 27:1797–1808. https://doi.org/10.1091/mbc.E15-07-0489

Barua, M., E.J. Brown, V.T. Charoonratana, G. Genovese, H. Sun, and M.R. Pollak. 2013. Mutations in the INF2 gene account for a significant proportion of familial but not sporadic focal and segmental glomerulosclerosis. *Kidney Int.* 83:316–322. https://doi.org/10.1038/ki.2012.349

Berbari, N.F., N. Sharma, E.B. Malarkey, J.N. Pieczynski, R. Boddu, J. Gaertig, L. Guay-Woodford, and B.K. Yoder. 2013. Microtubule modifications and stability are altered by cilia perturbation and in cystic kidney disease. *Cytoskeleton (Hoboken).* 70:24–31. https://doi.org/10.1002/cm.21088

Bouchet-Marquis, C., B. Zuber, A.-M. Glynn, M. Eltsov, M. Grabenbauer, K.N. Goldie, D. Thomas, A.S. Frangakis, J. Dubochet, and D. Chrétien. 2007. Visualization of cell microtubules in their native state. *Biol. Cell.* 99:45–53. https://doi.org/10.1042/BC20060081

Boyer, O., F. Nevo, E. Plaisier, B. Funalot, O. Gribouval, G. Benoit, E. Huynh Cong, C. Arrondel, M.-J. Tête, R. Montjean, et al. 2011. INF2 mutations in Charcot-Marie-Tooth disease with glomerulopathy. *N. Engl. J. Med.* 365:2377–2388. https://doi.org/10.1056/NEJMoa1109122

Brown, E.J., J.S. Schlöndorff, D.J. Becker, H. Tsukaguchi, S.J. Tonna, A.L. Uscinski, H.N. Higgs, J.M. Henderson, and M.R. Pollak. 2010. Mutations in the formin gene INF2 cause focal segmental glomerulosclerosis. *Nat. Genet.* 42:72–76. https://doi.org/10.1038/ng.505

Burton, P.R. 1984. Luminal material in microtubules of frog olfactory axons: Structure and distribution. *J. Cell Biol.* 99:520–528. https://doi.org/10.1083/jcb.99.2.520

Chen, J.K., J. Taipale, M.K. Cooper, and P.A. Beachy. 2002. Inhibition of Hedgehog signaling by direct binding of cyclopamine to Smoothened. *Genes Dev.* 16:2743–2748. https://doi.org/10.1101/gad.1025302

Cheng, L., J. Zhang, S. Ahmad, L. Rozier, H. Yu, H. Deng, and Y. Mao. 2011. Aurora B regulates formin mDia3 in achieving metaphase chromosome alignment. *Dev. Cell.* 20:342–352. https://doi.org/10.1016/j.devcel.2011.01.008

Chesarone, M.A., A.G. DuPage, and B.L. Goode. 2010. Unleashing formins to remodel the actin and microtubule cytoskeletons. *Nat. Rev. Mol. Cell Biol.* 11:62–74. https://doi.org/10.1038/nrm2816

Chhabra, E.S., and H.N. Higgs. 2006. INF2 Is a WASP homology 2 motif-containing formin that severs actin filaments and accelerates both polymerization and depolymerization. *J. Biol. Chem.* 281:26754–26767. https://doi.org/10.1074/jbc.M604666200

Chhabra, E.S., V. Ramabhadran, S.A. Gerber, and H.N. Higgs. 2009. INF2 is an endoplasmic reticulum-associated formin protein. *J. Cell Sci.* 122:1430–1440. https://doi.org/10.1242/jcs.040691

Copeland, J.W., and R. Treisman. 2002. The diaphanous-related formin mDia1 controls serum response factor activity through its effects on actin polymerization. *Mol. Biol. Cell.* 13:4088–4099. https://doi.org/10.1091/mbc.02-06-0092

Copeland, J.W., S.J. Copeland, and R. Treisman. 2004. Homo-oligomerization is essential for F-actin assembly by the formin family FH2 domain. *J. Biol. Chem.* 279:50250–50256. https://doi.org/10.1074/jbc.M404429200

d'Ydewalle, C., J. Krishnan, D.M. Chiheb, P. Van Damme, J. Irobi, A.P. Kozikowski, P. Vanden Berghe, V. Timmerman, W. Robberecht, and L. Van Den Bosch. 2011. HDAC6 inhibitors reverse axonal loss in a mouse model of mutant HSPB1-induced Charcot-Marie-Tooth disease. *Nat. Med.* 17:968–974. https://doi.org/10.1038/nm.2396

Dompierre, J.P., J.D. Godin, B.C. Charrin, F.P. Cordelières, S.J. King, S. Humbert, and F. Saudou. 2007. Histone deacetylase 6 inhibition compensates for the transport deficit in Huntington's disease by increasing tubulin acetylation. *J. Neurosci.* 27:3571–3583. https://doi.org/10.1523/JNEUROSCI.0037-07.2007

Esnault, C., A. Stewart, F. Gualdrini, P. East, S. Horswell, N. Matthews, and R. Treisman. 2014. Rho-actin signaling to the MRTF coactivators dominates the immediate transcriptional response to serum in fibroblasts. *Genes Dev.* 28:943–958. https://doi.org/10.1101/gad.239327.114

Etienne-Manneville, S. 2013. Microtubules in cell migration. *Annu. Rev. Cell Dev. Biol.* 29:471–499. https://doi.org/10.1146/annurev-cellbio-101011-155711

Gaillard, J., V. Ramabhadran, E. Neumanne, P. Gurel, L. Blanchoin, M. Vantard, and H.N. Higgs. 2011. Differential interactions of the formins INF2, mDia1, and mDia2 with microtubules. *Mol. Biol. Cell.* 22:4575–4587. https://doi.org/10.1091/mbc.E11-07-0616

Garvalov, B.K., B. Zuber, C. Bouchet-Marquis, M. Kudryashev, M. Gruska, M. Beck, A. Leis, F. Frischknecht, F. Bradke, W. Baumeister, et al. 2006. Luminal particles within cellular microtubules. *J. Cell Biol.* 174:759–765. https://doi.org/10.1083/jcb.200606074

Goode, B.L., and M.J. Eck. 2007. Mechanism and function of formins in the control of actin assembly. *Annu. Rev. Biochem.* 76:593–627. https://doi.org/10.1146/annurev.biochem.75.103004.142647

Green, R.A., E. Paluch, and K. Oegema. 2012. Cytokinesis in animal cells. *Annu. Rev. Cell Dev. Biol.* 28:29–58. https://doi.org/10.1146/annurev-cellbio-101011-155718

Gualdrini, F., C. Esnault, S. Horswell, A. Stewart, N. Matthews, and R. Treisman. 2016. SRF co-factors control the balance between cell proliferation and contractility. *Mol. Cell.* 64:1048–1061. https://doi.org/10.1016/j.molcel.2016.10.016

Guettler, S., M.K. Vartiainen, F. Miralles, B. Larijani, and R. Treisman. 2008. RPEL motifs link the serum response factor cofactor MAL but not myocardin to Rho signaling via actin binding. *Mol. Cell. Biol.* 28:732–742. https://doi.org/10.1128/MCB.01623-07

Haggarty, S.J., K.M. Koeller, J.C. Wong, C.M. Grozinger, and S.L. Schreiber. 2003. Domain-selective small-molecule inhibitor of histone deacetylase 6 (HDAC6)-mediated tubulin deacetylation. *Proc. Natl. Acad. Sci. USA.* 100:4389–4394. https://doi.org/10.1073/pnas.0430973100

Hammond, J.W., C.-F. Huang, S. Kaech, C. Jacobson, G. Banker, and K.J. Verhey. 2010. Posttranslational modifications of tubulin and the polarized transport of kinesin-1 in neurons. *Mol. Biol. Cell.* 21:572–583. https://doi.org/10.1091/mbc.E09-01-0044

Harris, E.S., I. Rouiller, D. Hanein, and H.N. Higgs. 2006. Mechanistic differences in actin bundling activity of two mammalian formins, FRL1 and mDia2. *J. Biol. Chem.* 281:14383–14392. https://doi.org/10.1074/jbc.M510923200

Howes, S.C., G.M. Alushin, T. Shida, M.V. Nachury, and E. Nogales. 2014. Effects of tubulin acetylation and tubulin acetyltransferase binding on microtubule structure. *Mol. Biol. Cell.* 25:257–266. https://doi.org/10.1091/mbc.E13-07-0387

Ishizaki, T., Y. Morishima, M. Okamoto, T. Furuyashiki, T. Kato, and S. Narumiya. 2001. Coordination of microtubules and the actin cytoskeleton by the Rho effector mDia1. *Nat. Cell Biol.* 3:8–14. https://doi.org/10.1038/35050598

Janke, C., and J.C. Bulinski. 2011. Post-translational regulation of the microtubule cytoskeleton: Mechanisms and functions. *Nat. Rev. Mol. Cell Biol.* 12:773–786. https://doi.org/10.1038/nrm3227

Jin, X., J. Wang, K. Gao, P. Zhang, L. Yao, Y. Tang, L. Tang, J. Ma, J. Xiao, E. Zhang, et al. 2017. Dysregulation of INF2-mediated mitochondrial fission in SPOP-mutated prostate cancer. *PLoS Genet.* 13:e1006748. https://doi.org/10.1371/journal.pgen.1006748

Kalebic, N., S. Sorrentino, E. Perlas, G. Bolasco, C. Martinez, and P.A. Heppenstall. 2013. αTAT1 is the major α-tubulin acetyltransferase in mice. *Nat. Commun.* 4:1962. https://doi.org/10.1038/ncomms2962

Kazantsev, A.G., and L.M. Thompson. 2008. Therapeutic application of histone deacetylase inhibitors for central nervous system disorders. *Nat. Rev. Drug Discov.* 7:854–868. https://doi.org/10.1038/nrd2681

Kim, G.-W., L. Li, M. Gorbani, L. You, and X.-J. Yang. 2013. Mice lacking α-tubulin acetyltransferase 1 are viable but display α-tubulin acetylation deficiency and dentate gyrus distortion. *J. Biol. Chem.* 288:20334–20350. https://doi.org/10.1074/jbc.M113.464792

Kim, J., J.E. Lee, S. Heynen-Genel, E. Suyama, K. Ono, K. Lee, T. Ideker, P. Aza-Blanc, and J.G. Gleeson. 2010. Functional genomic screen for modulators of ciliogenesis and cilium length. *Nature.* 464:1048–1051. https://doi.org/10.1038/nature08895

Konishi, Y., and M. Setou. 2009. Tubulin tyrosination navigates the kinesin-1 motor domain to axons. *Nat. Neurosci.* 12:559–567. https://doi.org/10.1038/nn.2314

Korobova, F., V. Ramabhadran, and H.N. Higgs. 2013. An actin-dependent step in mitochondrial fission mediated by the ER-associated formin INF2. *Science.* 339:464–467. https://doi.org/10.1126/science.1228360

Kreitzer, G., G. Liao, and G.G. Gundersen. 1999. Detyrosination of tubulin regulates the interaction of intermediate filaments with microtubules in vivo via a kinesin-dependent mechanism. *Mol. Biol. Cell.* 10:1105–1118. https://doi.org/10.1091/mbc.10.4.1105

L'Hernault, S.W., and J.L. Rosenbaum. 1985. Chlamydomonas alpha-tubulin is posttranslationally modified by acetylation on the epsilon-amino group of a lysine. *Biochemistry.* 24:473–478. https://doi.org/10.1021/bi00323a034

LeDizet, M., and G. Piperno. 1987. Identification of an acetylation site of Chlamydomonas alpha-tubulin. *Proc. Natl. Acad. Sci. USA.* 84:5720–5724. https://doi.org/10.1073/pnas.84.16.5720

Leung, S., and N.G. Miyamoto. 1989. Point mutational analysis of the human c-fos serum response factor binding site. *Nucleic Acids Res.* 17:1177–1195. https://doi.org/10.1093/nar/17.3.1177

Li, F., and H.N. Higgs. 2003. The mouse Formin mDia1 is a potent actin nucleation factor regulated by autoinhibition. *Curr. Biol.* 13:1335–1340. https://doi.org/10.1016/S0960-9822(03)00540-2

Li, L., and X.-J. Yang. 2015. Tubulin acetylation: Responsible enzymes, biological functions and human diseases. *Cell. Mol. Life Sci.* 72:4237–4255. https://doi.org/10.1007/s00018-015-2000-5

Lin, S.X., G.G. Gundersen, and F.R. Maxfield. 2002. Export from pericentriolar endocytic recycling compartment to cell surface depends on stable, detyrosinated (glu) microtubules and kinesin. *Mol. Biol. Cell.* 13:96–109. https://doi.org/10.1091/mbc.01-05-0224

Madrid, R., J.F. Aranda, A.E. Rodríguez-Fraticelli, L. Ventimiglia, L. Andrés-Delgado, M. Shehata, S. Fanayan, H. Shahheydari, S. Gómez, A. Jiménez, et al. 2010. The formin INF2 regulates basolateral-to-apical transcytosis and lumen formation in association with Cdc42 and MAL2. *Dev. Cell.* 18:814–827. https://doi.org/10.1016/j.devcel.2010.04.001

Manor, U., S. Bartholomew, G. Golani, E. Christenson, M. Kozlov, H. Higgs, J. Spudich, and J. Lippincott-Schwartz. 2015. A mitochondria-anchored isoform of the actin-nucleating spire protein regulates mitochondrial division. *eLife.* 4:e08828. https://doi.org/10.7554/eLife.08828

Miralles, F., G. Posern, A.-I. Zaromytidou, and R. Treisman. 2003. Actin dynamics control SRF activity by regulation of its coactivator MAL. *Cell.* 113:329–342. https://doi.org/10.1016/S0092-8674(03)00278-2

Morley, S.J., Y. Qi, L. Iovino, L. Andolfi, D. Guo, N. Kalebic, L. Castaldi, C. Tischer, C. Portulano, G. Bolasco, et al. 2016. Acetylated tubulin is essential for touch sensation in mice. *eLife.* 5:e20813. https://doi.org/10.7554/eLife.20813

Muehlich, S., R. Wang, S.-M. Lee, T.C. Lewis, C. Dai, and R. Prywes. 2008. Serum-induced phosphorylation of the serum response factor coactivator MKL1 by the extracellular signal-regulated kinase 1/2 pathway inhibits its nuclear localization. *Mol. Cell. Biol.* 28:6302–6313. https://doi.org/10.1128/MCB.00427-08

Nogales, E., M. Whittaker, R.A. Milligan, and K.H. Downing. 1999. High-resolution model of the microtubule. *Cell.* 96:79–88. https://doi.org/10.1016/S0092-8674(00)80961-7

Olson, E.N., and A. Nordheim. 2010. Linking actin dynamics and gene transcription to drive cellular motile functions. *Nat. Rev. Mol. Cell Biol.* 11:353–365. https://doi.org/10.1038/nrm2890

Palazzo, A.F., T.A. Cook, A.S. Alberts, and G.G. Gundersen. 2001. mDia mediates Rho-regulated formation and orientation of stable microtubules. *Nat. Cell Biol.* 3:723–729. https://doi.org/10.1038/35087035

Palazzo, A., B. Ackerman, and G.G. Gundersen. 2003. Cell biology (Communication arising): Tubulin acetylation and cell motility. *Nature.* 421:230. https://doi.org/10.1038/421230a

Panzer, L., L. Trübe, M. Klose, B. Joosten, J. Slotman, A. Cambi, and S. Linder. 2016. The formins FHOD1 and INF2 regulate inter- and intra-structural contractility of podosomes. *J. Cell Sci.* 129:298–313. https://doi.org/10.1242/jcs.177691

Perdiz, D., R. Mackeh, C. Poüs, and A. Baillet. 2011. The ins and outs of tubulin acetylation: More than just a post-translational modification? *Cell. Signal.* 23:763–771. https://doi.org/10.1016/j.cellsig.2010.10.014

Piperno, G., M. LeDizet, and X.J. Chang. 1987. Microtubules containing acetylated α-tubulin in mammalian cells in culture. *J. Cell Biol.* 104:289–302. https://doi.org/10.1083/jcb.104.2.289

Portran, D., L. Schaedel, Z. Xu, M. Théry, and M.V. Nachury. 2017. Tubulin acetylation protects long-lived microtubules against mechanical ageing. *Nat. Cell Biol.* 19:391–398. https://doi.org/10.1038/ncb3481

Posern, G., and R. Treisman. 2006. Actin' together: Serum response factor, its cofactors and the link to signal transduction. *Trends Cell Biol.* 16:588–596. https://doi.org/10.1016/j.tcb.2006.09.008

Prywes, R., and R.G. Roeder. 1987. Purification of the c-fos enhancer-binding protein. *Mol. Cell. Biol.* 7:3482–3489. https://doi.org/10.1128/MCB.7.10.3482

Qu, X., F.N. Yuan, C. Corona, S. Pasini, M.E. Pero, G.G. Gundersen, M.L. Shelanski, and F. Bartolini. 2017. Stabilization of dynamic microtubules by mDia1 drives Tau-dependent $A\beta_{1-42}$ synaptotoxicity. *J. Cell Biol.* 216:3161–3178. https://doi.org/10.1083/jcb.201701045

Ramabhadran, V., F. Korobova, G.J. Rahme, and H.N. Higgs. 2011. Splice variant-specific cellular function of the formin INF2 in maintenance of Golgi architecture. *Mol. Biol. Cell.* 22:4822–4833. https://doi.org/10.1091/mbc.E11-05-0457

Ramabhadran, V., P.S. Gurel, and H.N. Higgs. 2012. Mutations to the formin homology 2 domain of INF2 protein have unexpected effects on actin polymerization and severing. *J. Biol. Chem.* 287:34234–34245. https://doi.org/10.1074/jbc.M112.365122

Ramabhadran, V., A.L. Hatch, and H.N. Higgs. 2013. Actin monomers activate inverted formin 2 by competing with its autoinhibitory interaction. *J. Biol. Chem.* 288:26847–26855. https://doi.org/10.1074/jbc.M113.472415

Ran, F.A., P.D. Hsu, J. Wright, V. Agarwala, D.A. Scott, and F. Zhang. 2013. Genome engineering using the CRISPR-Cas9 system. *Nat. Protoc.* 8:2281–2308. https://doi.org/10.1038/nprot.2013.143

Reed, N.A., D. Cai, T.L. Blasius, G.T. Jih, E. Meyhofer, J. Gaertig, and K.J. Verhey. 2006. Microtubule acetylation promotes kinesin-1 binding and transport. *Curr. Biol.* 16:2166–2172. https://doi.org/10.1016/j.cub.2006.09.014

Rizvi, S.A., E.M. Neidt, J. Cui, Z. Feiger, C.T. Skau, M.L. Gardel, S.A. Kozmin, and D.R. Kovar. 2009. Identification and characterization of a small molecule inhibitor of formin-mediated actin assembly. *Chem. Biol.* 16:1158–1168. https://doi.org/10.1016/j.chembiol.2009.10.006

Seth, A., C. Otomo, and M.K. Rosen. 2006. Autoinhibition regulates cellular localization and actin assembly activity of the diaphanous-related formins FRLα and mDia1. *J. Cell Biol.* 174:701–713. https://doi.org/10.1083/jcb.200605006

Shao, X., Q. Li, A. Mogilner, A.D. Bershadsky, and G.V. Shivashankar. 2015. Mechanical stimulation induces formin-dependent assembly of a perinuclear actin rim. *Proc. Natl. Acad. Sci. USA.* 112:E2595–E2601. https://doi.org/10.1073/pnas.1504837112

Shaye, D.D., and I. Greenwald. 2015. The disease-associated formin INF2/EXC-6 organizes lumen and cell outgrowth during tubulogenesis by regulating F-actin and microtubule cytoskeletons. *Dev. Cell.* 32:743–755. https://doi.org/10.1016/j.devcel.2015.01.009

Shida, T., J.G. Cueva, Z. Xu, M.B. Goodman, and M.V. Nachury. 2010. The major α-tubulin K40 acetyltransferase alphaTAT1 promotes rapid ciliogenesis and efficient mechanosensation. *Proc. Natl. Acad. Sci. USA.* 107:21517–21522. https://doi.org/10.1073/pnas.1013728107

Skau, C.T., S.V. Plotnikov, A.D. Doyle, and C.M. Waterman. 2015. Inverted formin 2 in focal adhesions promotes dorsal stress fiber and fibrillar adhesion formation to drive extracellular matrix assembly. *Proc. Natl. Acad. Sci. USA.* 112:E2447–E2456. https://doi.org/10.1073/pnas.1505035112

Sun, Q., G. Chen, J.W. Streb, X. Long, Y. Yang, C.J. Stoeckert Jr., and J.M. Miano. 2006. Defining the mammalian CArGome. *Genome Res.* 16:197–207. https://doi.org/10.1101/gr.4108706

Thurston, S.F., W.A. Kulacz, S. Shaikh, J.M. Lee, and J.W. Copeland. 2012. The ability to induce microtubule acetylation is a general feature of formin proteins. *PLoS One.* 7:e48041. https://doi.org/10.1371/journal.pone.0048041

Tominaga, T., E. Sahai, P. Chardin, F. McCormick, S.A. Courtneidge, and A.S. Alberts. 2000. Diaphanous-related formins bridge Rho GTPase and Src tyrosine kinase signaling. *Mol. Cell.* 5:13–25. https://doi.org/10.1016/S1097-2765(00)80399-8

Treisman, R. 1987. Identification and purification of a polypeptide that binds to the c-fos serum response element. *EMBO J.* 6:2711–2717.

Wales, P., C.E. Schuberth, R. Aufschnaiter, J. Fels, I. García-Aguilar, A. Janning, C.P. Dlugos, M. Schäfer-Herte, C. Klingner, M. Wälte, et al. 2016. Calcium-mediated actin reset (CaAR) mediates acute cell adaptations. *eLife.* 5:e19850. https://doi.org/10.7554/eLife.19850

Wallar, B.J., and A.S. Alberts. 2003. The formins: Active scaffolds that remodel the cytoskeleton. *Trends Cell Biol.* 13:435–446. https://doi.org/10.1016/S0962-8924(03)00153-3

Wloga, D., and J. Gaertig. 2010. Post-translational modifications of microtubules. *J. Cell Sci.* 123:3447–3455. https://doi.org/10.1242/jcs.063727

Xu, Y., J.B. Moseley, I. Sagot, F. Poy, D. Pellman, B.L. Goode, and M.J. Eck. 2004. Crystal structures of a Formin Homology-2 domain reveal a tethered dimer architecture. *Cell.* 116:711–723. https://doi.org/10.1016/S0092-8674(04)00210-7

Xu, Z., L. Schaedel, D. Portran, A. Aguilar, J. Gaillard, M.P. Marinkovich, M. Théry, and M.V. Nachury. 2017. Microtubules acquire resistance from mechanical breakage through intralumenal acetylation. *Science.* 356:328–332. https://doi.org/10.1126/science.aai8764

Young, K.G., S.F. Thurston, S. Copeland, C. Smallwood, and J.W. Copeland. 2008. INF1 is a novel microtubule-associated formin. *Mol. Biol. Cell.* 19:5168–5180. https://doi.org/10.1091/mbc.E08-05-0469

Zhou, F., P. Leder, and S.S. Martin. 2006. Formin-1 protein associates with microtubules through a peptide domain encoded by exon-2. *Exp. Cell Res.* 312:1119–1126. https://doi.org/10.1016/j.yexcr.2005.12.035